

On the Input-Output Behavior of a Geothermal Energy Storage: Approximations by Model Order Reduction

Paul Honore Takam · Ralf Wunderlich

Abstract In this paper we consider a geothermal energy storage in which the spatio-temporal temperature distribution is modeled by a heat equation with a convection term. Such storages often are embedded in residential heating systems and control and management require the knowledge of some aggregated characteristics of that temperature distribution in the storage. They describe the input-output behaviour of the storage and the associated energy flows and their response to charging and discharging processes. We aim to derive an efficient approximative description of these characteristics by a low-dimensional system of ODEs. This leads to a model order reduction problem for a large scale linear system of ODEs arising from the semi-discretization of the heat equation combined with a linear algebraic output equation. In a first step we approximate the non time-invariant system of ODEs by a linear time-invariant system. Then we apply Lyapunov balanced truncation model order reduction to approximate the output by a reduced-order system with only a few state equations but almost the same input-output behavior. The paper presents results of extensive numerical experiments showing the efficiency of the applied model order reduction methods. It turns out that only a few suitable chosen ODEs are sufficient to produce good approximations of the input-output behaviour of the storage.

Keywords Geothermal energy storage · Heat equation · Large-scale systems · Model order reduction · Lyapunov balanced truncation · Gramians

Mathematics Subject Classification (2010) 93A15 · 93B11 · 93C05 · 93C15 · 37M99

1 Introduction

Heating and cooling systems of single buildings as well as for district heating systems manage and mitigate temporal fluctuations of heat supply and demand by using thermal storage facilities. They allow thermal energy to be stored and to be used hours, days, weeks or months later. This is attractive for space heating, domestic or process hot water production, or generating electricity. Note that thermal energy may also be stored in the way of cold. Thermal storages can significantly increase both the flexibility and the performance of district energy systems and enhancing the integration of intermittent renewable energy sources into thermal networks (see Guelpa and Verda [19], Kitapbayev et al. [26]).

Paul Honore Takam / Ralf Wunderlich

Brandenburg University of Technology Cottbus-Senftenberg, Institute of Mathematics, P.O. Box 101344, 03013 Cottbus, Germany; E-mail: takam@b-tu.de / ralf.wunderlich@b-tu.de

Geothermal storages constitute an important class of thermal storages and enable an extremely efficient operation of heating and cooling systems in buildings. Further, they can be used to mitigate peaks in the electricity grid by converting electrical into heat energy (power to heat). Pooling several geothermal storages within the framework of a virtual power plant gives the necessary capacity which allows to participate in the balancing energy market.

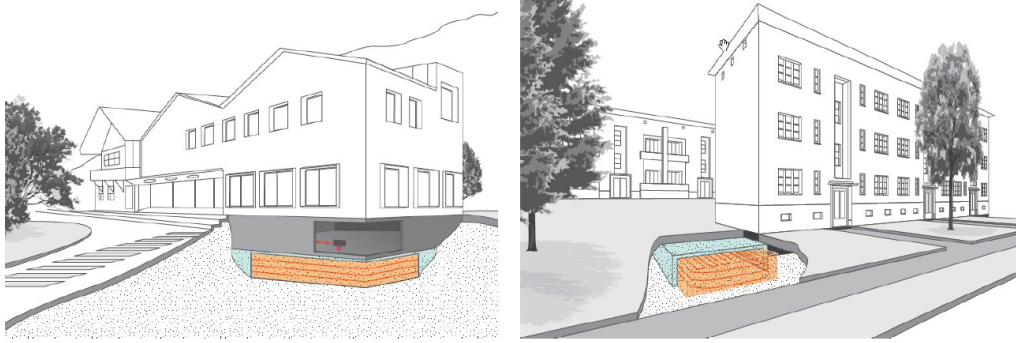


Fig. 1.1 Geothermal storage: in the new building, under a building (left) and in the renovation, aside of the building (right), see www.ezeit-ingenieure.eu, www.geo-ec.de.

The present paper considers geothermal storages as depicted in Fig.1.1 and presented in detail in our companion papers [37,38]. Such storages gain more and more importance and are quite attractive for residential heating systems since construction and maintenance are relatively inexpensive. Furthermore, they can be integrated both in new buildings and in renovations. For the storage a defined volume is filled with soil and insulated to the surrounding ground. The thermal energy is stored by raising the temperature of the soil inside the storage. It is charged and discharged via pipe heat exchangers (PHX) filled with some fluid such as water. These PHXs are connected to a residential heating system, in particular to internal storages such as water tanks, or directly to a solar collector. The fluid carrying the thermal energy is moved by pumps and heat pumps where the latter raise the temperature to a higher level using electrical energy.

A special feature of the considered geothermal storage is that it is not insulated at the bottom such that thermal energy can also flow into deeper layers as it can be seen in Fig. 1.2. This allows for an extension of the storage capacity since that heat can to some extent be retrieved if the storage is sufficiently discharged (cooled) and a heat flux back to storage is induced. The unavoidable losses due to the diffusion to the environment can be compensated since such geothermal storages can benefit from higher temperatures in deeper layers of the ground and therefore also serve as a production units similar to downhole heat exchangers. This becomes interesting during winter since in many regions in Europe the temperature in a depth of only 10 meter over the year is almost constant around 10°C .

For the operation of a geothermal storage within a residential system the controller or manager of that system need to know certain aggregated characteristics of the spatial temperature distribution in the storage, their dynamics and response to charging and discharging decisions. Note that the latter means to decide if the fluid is pumped through the PHXs to the storage or if it is at rest and pumps are off. Further, if pumps are on one has to decide on an appropriate temperature of the fluid. An example of such an aggregated

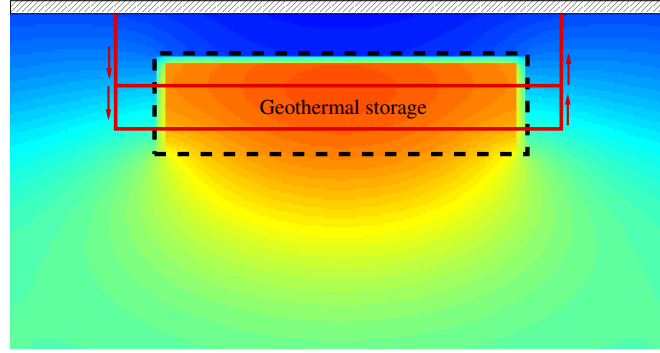


Fig. 1.2 2D-model of a geothermal storage insulated to the top and the sides (green bars) while open to the bottom and spatial temperature distribution.

characteristic is the average temperature in the storage medium from which one can derive the amount of available thermal energy that can be stored in or extracted from the storage. Another example is the average temperature at the outlet which allows to determine the amount of energy injected to or withdrawn from the storage. Further, the average temperature at the bottom of the storage allows to quantify the heat transfer to and from the ground via the open bottom boundary. For more details we refer to Sec. 4.

The above aggregated characteristics can be computed by postprocessing the spatio-temporal temperature distribution in the storage. The latter can be obtained by solving the governing linear heat equation with convection and appropriate boundary and interface conditions. This is explained in Secs. 2 and 3. There we work with a 2D model of the storage and use finite difference methods for the semi-discretization of the PDE w.r.t the spatial variables. That approach is also known as 'method of lines' and leads to a high-dimensional system of ODEs. We refer to our companion papers [37,38] for details and a stability analysis of the finite difference scheme as well as results of extensive numerical experiments. Further, we refer to a previous study in Bähr et al. [3,4] where the storage was not considered isolated but embedded in the surrounding domain and the interaction between geothermal storage and the environment was studied. In that papers the focus was on the numerical simulation of the long-term behaviour of the spatial temperature distribution. For simplicity charging and discharging was described by a simple source term but not by PHXs. The focus of the present paper is on the computation of the short-term behaviour of the spatial temperature distribution and its response to charging and discharging processes. We choose the computational domain to be the storage depicted in Fig. 1.2 by a dashed black rectangle. For the sake of simplicity we do not consider the surrounding medium but set appropriate boundary conditions to mimic the interaction between storage and environment. In addition to [3,4] we model PHXs which are used to charge and discharge the storage.

The cost-optimal management of residential heating systems equipped with a geothermal storage can be treated mathematically in terms of optimal control problems. This requires to model the input-output behavior of the storage, i.e. the dynamics of the above mentioned aggregated characteristics and their response to charging and discharging processes. Working with the governing PDE for the heat propagation or an approximating high-dimensional system of ODEs becomes then intractable due to the curse of dimensionality. Therefore one wishes to describe the input-out behavior of the storage by a suitable

low-dimensional system of ODEs with a sufficiently high approximation accuracy. This leads to a problem of model order reduction which is the focus in the present paper.

In our model assumptions in Sec. 2 we restrict to the case of a piecewise constant velocity of the fluid in the PHXs. This is often observed in real-world systems which operate with constant velocity during charging and discharging if pumps are on while the velocity is zero if pumps are off. Then the high-dimensional system of ODEs constitutes a system of n linear non-autonomous ODEs since the system matrices depend on time via the fluid velocity. The latter varies over time and is only piecewise constant. Thus, the obtained linear system is not linear time-invariant (LTI). The latter is a crucial assumption for many of model reduction methods. In Sec. 5 we circumvent this problem by approximating the model for the geothermal storage by a so-called *analogous model* which is LTI. The key idea for the construction of such an analogue is to mimic the original model by a LTI system where pumps are always on such that the fluid velocity is constant all the time. During the waiting periods we use at the inlet and outlet boundary the same type of boundary conditions as during charging and discharging. However, we choose the inlet temperature to be equal to the average temperature in the PHX. Numerical examples presented in [38] show that the analogous system approximates the original system quite well.

For the derived linear LTI system we apply in Sec. 6 the Lyapunov balanced truncation model order reduction method which is well suited for our purposes. It was first introduced by Mullis and Roberts [30] and later in the linear systems and control literature by Moore [29]. The idea of that method is first, to transform the system into an appropriate coordinate system for the state-space in which the states that are difficult to reach, that is, require a large input energy to be reached. They are simultaneously difficult to observe, i.e., produce a small observation output energy. Then, the reduced model is obtained by truncating the states which are simultaneously difficult to reach and to observe. Among the various model order reduction methods balanced truncation is characterized by the preservation of several system properties like stability and passivity, see Pernebo and Silverman [32]. Further, it provides error bounds that permit an appropriate choice of the dimension of the reduced-order model depending on the desired accuracy of the approximation, see Enns [15].

Besides the Lyapunov balancing method, there exist other types of balancing techniques such as stochastic balancing, bounded real balancing, positive real balancing and frequency weighted balancing, see Antoulas [2] and Gugercin and Antoulas [20]. Gosea et al. [18] considers balanced truncation for linear switched systems. In the book of Benner et al. [8], an efficient implementation of model reduction methods such as modal truncation, balanced truncation, and other balancing-related truncation techniques is presented. Further, the authors discussed various aspects of balancing-related techniques for large-scale systems, structured systems, and descriptor systems. The results presented in [8] also cover the model reduction techniques for time-varying as well as the model reduction for second- and higher-order systems, which can be considered as one of the major research directions in dimension reduction for linear systems. In addition, surveys on system approximation and model reduction can be found in [1, 2, 10, 11, 16, 20, 27, 28, 33, 40] and the references therein.

The rest of the paper is organized as follow. In Sec. 2 we describe the mathematical modeling of the geothermal storage. We present the heat equation with a convection term and appropriate boundary and interface conditions which governs the dynamics of the spatial temperature distribution in the storage. Sec. 3 is devoted to the finite difference

semi-discretization of the heat equation. In Sec. 4 we introduce aggregated characteristics of the spatio-temporal temperature distribution. Sec. 5 derives the approximate LTI analogous model of the geothermal storage. In Sec. 6 we start with the formulation of the general model reduction problem. Then we present the Lyapunov balanced truncation method. Sec. 7 presents results of various numerical experiments where the aggregated characteristics of the temperature distribution in storage for the original model are compared with the approximations obtained from reduced-order models. In Sec. 8 we present some conclusions. An appendix provides a list of frequently used notations and some proofs which were removed from the main text.

2 Dynamics of the Geothermal Storage

The setting is based on our companion paper [37, Sec. 2]. For self-containedness and the convenience of the reader, we recall in this section the description of the model. The dynamics of the spatial temperature distribution in a geothermal storage can be described mathematically by a linear heat equation with convection term and appropriate boundary and interface conditions.

2.1 2D-Model

We assume that the domain of the geothermal storage is a cuboid and consider a two-dimensional rectangular cross-section. We denote by $Q = Q(t, x, y)$ the temperature at time $t \in [0, T]$ in the point $(x, y) \in \mathcal{D} = (0, l_x) \times (0, l_y)$ with l_x, l_y denoting the width and height of the storage. The domain \mathcal{D} and its boundary $\partial\mathcal{D}$ are depicted in Fig. 2.1. \mathcal{D} is divided into three parts. The first is \mathcal{D}^M and filled with a homogeneous medium (soil) characterized by material parameters ρ^M, κ^M and c_p^M denoting mass density, thermal conductivity and specific heat capacity, respectively. The second is \mathcal{D}^F , it represents the PHXs and is filled with a fluid (water) with constant material parameters ρ^F, κ^F and c_p^F . The fluid moves with time-dependent velocity $v_0(t)$ along the PHXs. For the sake of simplicity we restrict to the case, often observed in applications, where the pumps moving the fluid are either on or off. Thus the velocity $v_0(t)$ is piecewise constant taking values $\bar{v}_0 > 0$ and zero, only. Finally, the third part is the interface \mathcal{D}^I between \mathcal{D}^M and \mathcal{D}^F . For the sake of simplicity we neglect modeling the wall of the PHX and suppose perfect contact between the PHX and the soil. Details are given below in (2.5) and (2.6). Summarizing we make the following

Assumption 2.1

1. *Material parameters of the medium ρ^M, κ^M, c_p^M in the domain \mathcal{D}^M and of the fluid ρ^F, κ^F, c_p^F in the domain \mathcal{D}^F are constants.*
2. *Fluid velocity is piecewise constant, i.e. $v_0(t) = \begin{cases} \bar{v}_0 > 0, & \text{pump on} \\ 0, & \text{pump off} \end{cases}$*
3. *Perfect contact at the interface between fluid and medium.*

Remark 2.2 Results obtained for our 2D-model, where \mathcal{D} represents the rectangular cross-section of a box-shaped storage can be extended to the 3D-case if we assume that the 3D

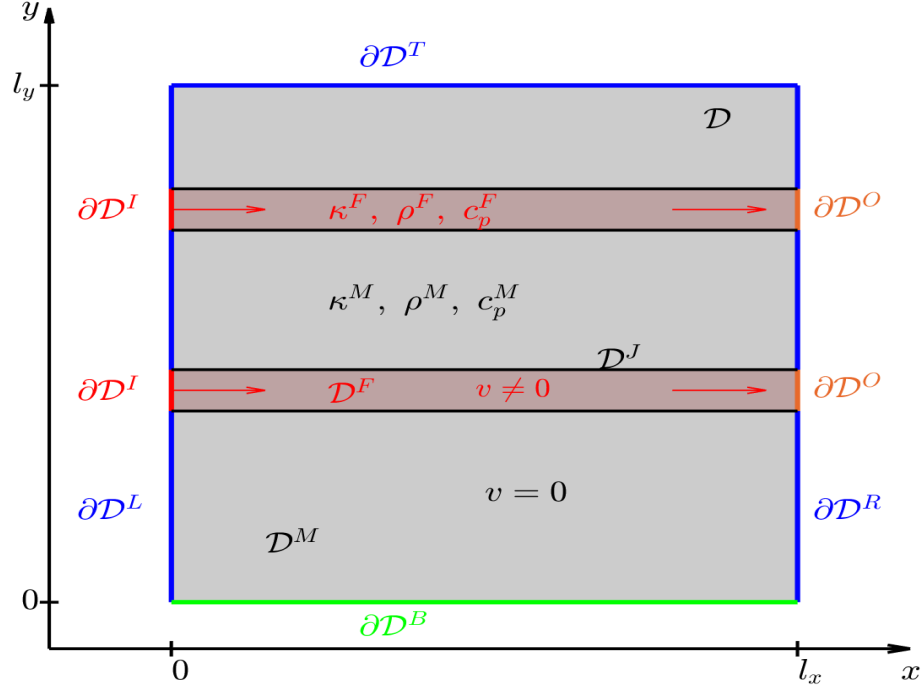


Fig. 2.1 2D-model of the geothermal storage: decomposition of the domain \mathcal{D} and the boundary $\partial\mathcal{D}$.

storage domain is a cuboid of depth l_z with an homogeneous temperature distribution in z -direction. A PHX in the 2D-model then represents a horizontal snake-shaped PHX densely filling a small layer of the storage.

Heat equation. The temperature $Q = Q(t, x, y)$ in the external storage is governed by the linear heat equation with convection term

$$\rho c_p \frac{\partial Q}{\partial t} = \nabla \cdot (\kappa \nabla Q) - \rho v \cdot \nabla (c_p Q), \quad (t, x, y) \in (0, T] \times \mathcal{D} \setminus \mathcal{D}^J,$$

where the first term on the right hand side describes diffusion while the second represents convection of the moving fluid in the PHXs. Further, $v = v(t, x, y) = v_0(t)(v^x(x, y), v^y(x, y))^\top$ denotes the velocity vector with $(v^x, v^y)^\top$ being the normalized directional vector of the flow. According to Assumption 2.1 the material parameters ρ, κ, c_p depend on the position (x, y) and take the values ρ^M, κ^M, c_p^M for points in \mathcal{D}^M (medium) and ρ^F, κ^F, c_p^F in \mathcal{D}^F (fluid).

Note that there are no sources or sinks inside the storage and therefore the above heat equation appears without forcing term. Based on this assumption, the heat equation (2.1) can be written as

$$\frac{\partial Q}{\partial t} = a \Delta Q - v \cdot \nabla Q, \quad (t, x, y) \in (0, T] \times \mathcal{D} \setminus \mathcal{D}^J, \quad (2.1)$$

where $\Delta = \frac{\partial^2}{\partial x^2} + \frac{\partial^2}{\partial y^2}$ is the Laplace operator, $\nabla = (\frac{\partial}{\partial x}, \frac{\partial}{\partial y})$ the gradient operator, and $a = a(x, y)$ is the thermal diffusivity which is piecewise constant with values $a^\dagger = \frac{\kappa^\dagger}{\rho^\dagger c_p^\dagger}$ with $\dagger = M$ for $(x, y) \in \mathcal{D}^M$ and $\dagger = F$ for $(x, y) \in \mathcal{D}^F$, respectively. The initial condition $Q(0, x, y) = Q_0(x, y)$ is given by the initial temperature distribution Q_0 of the storage.

2.2 Boundary and Interface Conditions

For the description of the boundary conditions we decompose the boundary $\partial\mathcal{D}$ into several subsets as depicted in Fig. 2.1 representing the insulation on the top and the side, the open bottom, the inlet and outlet of the PHXs. Further, we have to specify conditions at the interface between PHXs and soil. The inlet, outlet and the interface conditions model the heating and cooling of the storage via PHXs. We distinguish between the two regimes 'pump on' and 'pump off' where for simplicity we assume perfect insulation at inlet and outlet if the pump is off. This leads to the following boundary conditions.

- *Homogeneous Neumann condition* describing perfect insulation on the top and the side

$$\frac{\partial Q}{\partial \mathbf{n}} = 0, \quad (x, y) \in \partial\mathcal{D}^T \cup \partial\mathcal{D}^L \cup \partial\mathcal{D}^R, \quad (2.2)$$

where $\partial\mathcal{D}^L = \{0\} \times [0, l_y] \setminus \partial\mathcal{D}^I$, $\partial\mathcal{D}^R = \{l_x\} \times [0, l_y] \setminus \partial\mathcal{D}^O$, $\partial\mathcal{D}^T = [0, l_x] \times \{l_y\}$ and \mathbf{n} denotes the outer-pointing normal vector.

- *Robin condition* describing heat transfer on the bottom

$$-\kappa^M \frac{\partial Q}{\partial \mathbf{n}} = \lambda^G (Q - Q^G(t)), \quad (x, y) \in \partial\mathcal{D}^B, \quad (2.3)$$

with $\partial\mathcal{D}^B = (0, l_x) \times \{0\}$, where $\lambda^G > 0$ denotes the heat transfer coefficient and $Q^G(t)$ the underground temperature.

- *Dirichlet condition* at the inlet if the pump is on ($v_0(t) > 0$), i.e. the fluid arrives at the storage with a given temperature $Q^I(t)$. If the pump is off ($v_0(t) = 0$), we set a homogeneous Neumann condition describing perfect insulation.

$$\begin{cases} Q = Q^I(t), & \text{pump on,} \\ \frac{\partial Q}{\partial \mathbf{n}} = 0, & \text{pump off,} \end{cases} \quad (x, y) \in \partial\mathcal{D}^I. \quad (2.4)$$

- *“Do Nothing” condition* at the outlet in the following sense. If the pump is on ($v_0(t) > 0$) then the total heat flux directed outwards can be decomposed into a diffusive heat flux given by $k^f \frac{\partial Q}{\partial \mathbf{n}}$ and a convective heat flux given by $v_0(t) \rho^F c_p^F Q$. In our model we can neglect the diffusive heat flux. This leads to a homogeneous Neumann condition

$$\frac{\partial Q}{\partial \mathbf{n}} = 0, \quad (x, y) \in \partial\mathcal{D}^O.$$

If the pump is off then we assume perfect insulation which is also described by the above condition.

- *Smooth heat flux* at interface \mathcal{D}^J between fluid and soil leading to a coupling condition

$$\kappa^F \left(\frac{\partial Q^F}{\partial \mathbf{n}} \right) = \kappa^M \left(\frac{\partial Q^M}{\partial \mathbf{n}} \right), \quad (x, y) \in \mathcal{D}^J. \quad (2.5)$$

Here, Q^F, Q^M denote the temperature of the fluid inside the PHX and of the soil outside the PHX, respectively. Moreover, we assume that the contact between the PHX and the medium is perfect which leads to a smooth transition of a temperature, i.e., we have

$$Q^F = Q^M, \quad (x, y) \in \mathcal{D}^J. \quad (2.6)$$

3 Semi-Discretization of the Heat Equation

We now sketch the discretization of the heat equation (2.1) together with the boundary and interface conditions given in (2.2) through (2.6). For details we refer to our companion paper [37, Sec. 3]. We confine ourselves to a semi-discretization in space and approximate only spatial derivatives by their respective finite differences. This approach is also known as 'method of lines' and leads to a high-dimensional system of ODEs for the temperatures at the grid points. The latter will serve as starting point for the model reduction in Sec. 6. For the full discretization in which time is also discretized we refer to our companion paper [38, Sec. 4] where we derive an implicit finite difference scheme and study its stability.

3.1 Semi-Discretization of the Heat Equation

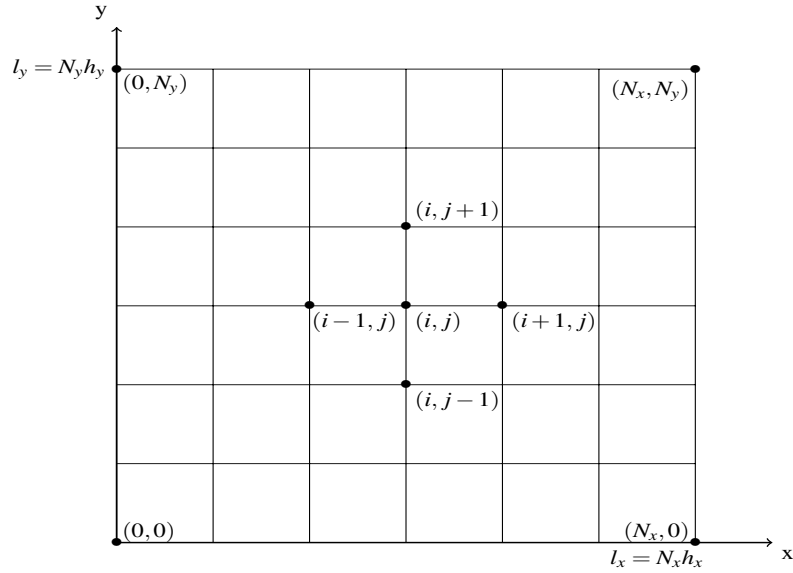


Fig. 3.1 Computational grid.

The spatial domain depicted in Fig. 2.1 is discretized by the means of a mesh with grid points (x_i, y_j) as in Fig. 3.1 where $x_i = ih_x$, $y_j = jh_y$, $i = 0, \dots, N_x$, $j = 0, \dots, N_y$. Here, N_x and N_y denote the the number of grid points while $h_x = l_x/N_x$ and $h_y = l_y/N_y$ are the step sizes in x and y -direction, respectively. We denote by $Q_{ij}(t) \simeq Q(t, x_i, y_j)$ the semi-discrete approximation of the temperature Q and by $v_0(t)(v_{ij}^x, v_{ij}^y)^\top = v_0(t)(v^x(x_i, y_j), v^y(x_i, y_j))^\top = v(t, x_i, y_j)$ the velocity vector at the grid point (x_i, y_j) at time t .

For the sake of simplification and tractability of our analysis we restrict to the following assumption on the arrangement of PHXs and impose conditions on the location of grid points along the PHXs.

Assumption 3.1

1. There are $n_P \in \mathbb{N}$ straight horizontal PHXs, the fluid moves in positive x -direction.
2. The diameter of the PHXs are such that the interior of PHXs contains grid points.

3. Each interface between medium and fluid contains grid points.

We approximate the spatial derivatives in the heat equation, the boundary and interface conditions by finite differences as in [37, Subsec. 3.1–3] where we apply upwind techniques for the convection terms. The result is the system of ODEs (3.1) (given below) for a vector function $Y : [0, T] \rightarrow \mathbb{R}^n$ collecting the semi-discrete approximations $Q_{ij}(t)$ of the temperature $Q(t, x_i, y_j)$ in the “inner” grid points, i.e., all grid points except those on the boundary $\partial\mathcal{D}$ and the interface \mathcal{D}^J . For a model with n_P PHXs the dimension of Y is $n = (N_x - 1)(N_y - 2n_P - 1)$, see [37].

Using the above notation the semi-discretized heat equation (2.1) together with the given initial, boundary and interface conditions reads as

$$\dot{Y}(t) = A(t)Y(t) + B(t)g(t), \quad t \in (0, T], \quad (3.1)$$

with the initial condition $Y(0) = y_0$ where the vector $y_0 \in \mathbb{R}^n$ contains the initial temperatures $Q_0(\cdot, \cdot)$ at the corresponding grid points. The system matrix A results from the spatial discretization of the convection and diffusion term in the heat equation (2.1) together with the Robin and linear heat flux boundary conditions. It has the tridiagonal structure

$$A = \begin{pmatrix} A_L & D^+ & & & 0 \\ D^- & A_M & D^+ & & \\ & D^- & A_M & D^+ & \\ & & \ddots & \ddots & \ddots \\ 0 & & & D^- & A_M & D^+ \\ & & & & D^- & A_R \end{pmatrix} \quad (3.2)$$

and consists of $(N_x - 1) \times (N_x - 1)$ block matrices of dimension $q = N_y - 2n_P - 1$. The block matrices A_L, A_M, A_R on the diagonal have a tridiagonal structure and are given in [37, Table 3.1 and B.1]. The block matrices on the subdiagonals $D^\pm \in \mathbb{R}^{q \times q}$, $i = 1, \dots, N_x - 1$, are diagonal matrices and given in [37, Eq. (3.12)].

As a result of the discretization of the Dirichlet condition at the inlet boundary and the Robin condition at the bottom boundary, we get the function $g : [0, T] \rightarrow \mathbb{R}^2$ called input function and the $n \times 2$ input matrix B called input matrix. The entries of the input matrix B_{lr} , $l = 1, \dots, n$, $r = 1, 2$, are derived in [37, Subsec 3.4] and are given by

$$B_{l1} = B_{l1}(t) = \begin{cases} \frac{a^F}{h_x^2} + \frac{\bar{v}_0}{h_x} & \text{pump on,} \\ 0 & \text{pump off,} \end{cases} \quad l = \mathcal{K}(1, j), (x_0, y_j) \in \mathcal{D}^I, \quad (3.3)$$

$$B_{l2} = \frac{\lambda^G h_y}{\kappa^M + \lambda^G h_y} \beta^M, \quad l = \mathcal{K}(i, 1), (x_i, y_0) \in \mathcal{D}^B,$$

with $\beta^M = a^M / h_y^2$. The entries for other l are zero. Here, \mathcal{K} denotes the mapping $(i, j) \mapsto l = \mathcal{K}(i, j)$ of pairs of indices of grid point $(x_i, y_j) \in \mathcal{D}$ to the single index $l \in \{1, \dots, n\}$ of the corresponding entry in the vector Y . The input function reads as

$$g(t) = \begin{cases} (Q^I(t), Q^G(t))^\top, & \text{pump on,} \\ (0, Q^G(t))^\top, & \text{pump off.} \end{cases} \quad (3.4)$$

Recall that Q^I is the inlet temperature of the pipe during pumping and Q^G is the under-ground temperature.

3.2 Stability of Matrix A

The finite difference semi-discretization of the heat equation (2.1) given by the system of ODEs (3.1) is expected to preserve the dissipativity of the PDE. This property is related to the stability of the system matrix $A = A(t)$ in the sense that all eigenvalues of A lie in left open complex half plane. That property will play a crucial role below in Sec. 6 where we study model reduction techniques for (3.1) based on balanced truncation. The next theorem confirms the expectations on the stability of A . For the proof we refer to our companion paper [37, Theorem 3.3].

Theorem 3.2 (Stability of Matrix A)

Under Assumption 2.1 on the model and Assumption 3.1 on the discretization, the matrix $A = A(t)$ given in (3.2) is stable for all $t \in [0, T]$, i.e., all eigenvalues $\lambda(A)$ of A lie in left open complex half plane.

4 Aggregated Characteristics

The numerical methods introduced in Sec. 3 allow the approximate computation of the spatio-temporal temperature distribution in the geothermal storage. In many applications it is not necessary to know the complete information about that distribution. An example is the management and control of a storage which is embedded into a residential heating system. Here it is sufficient to know only a few aggregated characteristics of the temperature distribution which can be computed via post-processing. In this section we introduce some of these aggregated characteristics and describe their approximate computation based on the solution vector Y of the finite difference scheme.

4.1 Aggregated Characteristics Related to the Amount of Stored Energy

We start with aggregated characteristics given by the average temperature in some given subdomain of the storage which are related to the amount of stored energy in that domain.

Let $\mathcal{B} \subset \mathcal{D}$ be a generic subset of the 2D computational domain. We denote by $|\mathcal{B}| = \iint_{\mathcal{B}} dx dy$ the area of \mathcal{B} . Then $W_{\mathcal{B}}(t) = l_z \iint_{\mathcal{B}} \rho c_p Q(t, x, y) dx dy$ represents the thermal energy contained in the 3D spatial domain $\mathcal{B} \times [0, l_z]$ at time $t \in [0, T]$. Then for $0 \leq t_0 < t_1 \leq T$ the difference $G_{\mathcal{B}}(t_0, t_1) = W_{\mathcal{B}}(t_1) - W_{\mathcal{B}}(t_0)$ is the gain of thermal energy during the period $[t_0, t_1]$. While positive values correspond to warming of \mathcal{B} , negative values indicate cooling and $-G_{\mathcal{B}}(t_0, t_1)$ represents the size of the loss of thermal energy.

For $\mathcal{B} = \mathcal{D}^{\dagger}$, $\dagger = M, F$, we can use that the material parameters on \mathcal{D}^{\dagger} equal the constants $\rho = \rho^{\dagger}$, $c_p = c_p^{\dagger}$. Thus, for the corresponding gain of thermal energy we obtain

$$\begin{aligned} G^{\dagger} &= G^{\dagger}(t_0, t_1) := G_{\mathcal{D}^{\dagger}}(t_0, t_1) = \rho^{\dagger} c_p^{\dagger} |\mathcal{D}^{\dagger}| l_z (\bar{Q}^{\dagger}(t_1) - \bar{Q}^{\dagger}(t_0)), \\ \text{where } \bar{Q}^{\dagger}(t) &= \frac{1}{|\mathcal{D}^{\dagger}|} \iint_{\mathcal{D}^{\dagger}} Q(t, x, y) dx dy, \quad \dagger = M, F, \end{aligned} \quad (4.1)$$

denotes the average temperature in the medium ($\dagger = M$) and the fluid ($\dagger = F$), respectively.

4.2 Aggregated Characteristics Related to the Heat Flux at the Boundary

Now we consider the convective heat flux at the inlet and outlet boundary and the heat transfer at the bottom boundary. Let $\mathcal{C} \subset \partial\mathcal{D}$ be a generic curve on the boundary, then we denote by $|\mathcal{C}| = \int_{\mathcal{C}} ds$ the curve length.

The rate at which the energy is injected or withdrawn via the PHX is given by

$$\begin{aligned} R^P(t) &= \rho^F c_p^F v_0(t) \left[\int_{\mathcal{D}^I} Q(t, x, y) ds - \int_{\mathcal{D}^O} Q(t, x, y) ds \right] \\ &= \rho^F c_p^F v_0(t) |\partial\mathcal{D}^O| [Q^I(t) - \bar{Q}^O(t)], \end{aligned} \quad (4.2)$$

where $\bar{Q}^O(t) = \frac{1}{|\partial\mathcal{D}^O|} \int_{\partial\mathcal{D}^O} Q(t, x, y) ds$

is the average temperature at the outlet boundary. Here, it is used that in our model we have horizontal PHXs such that $|\partial\mathcal{D}^I| = |\partial\mathcal{D}^O|$ and a uniformly distributed inlet temperature at the inlet boundary $\partial\mathcal{D}^I$. For a given interval of time $[t_0, t_1]$ the quantity

$$G^P = G^P(t_0, t_1) = l_z \int_{t_0}^{t_1} R^P(t) dt$$

describes the amount of heat injected ($G^P > 0$) to or withdrawn ($G^P < 0$) from the storage due to convection of the fluid. Note that the fluid moves at time t with velocity $v_0(t)$ and arrives at the inlet with temperature $Q^I(t)$ while it leaves at the outlet with the average temperature $\bar{Q}^O(t)$.

Next we look at the diffusive heat transfer via the bottom boundary and define the rate

$$\begin{aligned} R^B(t) &= \int_{\mathcal{D}^B} \kappa^M \frac{\partial Q}{\partial \mathbf{n}} ds = \int_{\mathcal{D}^B} \lambda^G (Q^G(t) - Q(t, x, y)) ds \\ &= \lambda^G |\partial\mathcal{D}^B| (Q^G(t) - \bar{Q}^B(t)), \end{aligned} \quad (4.3)$$

where $\bar{Q}^B(t) = \frac{1}{|\partial\mathcal{D}^B|} \int_{\partial\mathcal{D}^B} Q(t, x, y) ds$,

is the average temperature at the bottom boundary. Note that the second equation in the first line follows from the Robin boundary condition. The quantity

$$G^B = G^B(t_0, t_1) = l_z \int_{t_0}^{t_1} R^B(t) dt$$

describes the amount of heat transferred via the bottom boundary of the storage.

4.3 Numerical Computation of Aggregated Characteristics

For the numerical simulation of the aggregated characteristics introduced in the previous subsections these quantities have to be expressed in terms of the finite difference approximations of the temperature $Q = Q(t, x, y)$. Then one obtains approximations in terms of the entries of the vector function $Y(t)$ satisfying the system of ODEs (3.1) and containing the semi-discrete finite difference approximations of the temperature in the inner grid points of the computational domain \mathcal{D} . Recall that the temperatures on boundary and interface grid points can be determined by linear combinations from the entries of $Y(t)$.

Let $\bar{Q}^\dagger(t)$ be one of the average temperatures $\bar{Q}^M, \bar{Q}^F, \bar{Q}^O, \bar{Q}^B$. Then the numerical approximation of the defining single and double integrals by quadrature rules leads to approximations by linear combinations of the entries of Y of the form

$$\bar{Q}^\dagger(t) \approx C^\dagger Y(t) \quad (4.4)$$

where C^\dagger is some $1 \times n$ -matrix. For the details we refer to our companion paper [38, Subsection 4.2, Appendix B].

5 Analogous Linear Time-Invariant System

Eq. (3.1) represents a system of n linear non-autonomous ODEs. Since some of the entries in the matrices A and B resulting from the discretization of convection terms in the heat equation (2.1) depend on the velocity $v_0(t)$, it follows that A and B are time-dependent. Thus, (3.1) does not constitute a linear time-invariant (LTI) system. The latter is a crucial assumption for many of model reduction methods such as the Lyapunov balanced truncation technique that is considered below in Sec. 6. We circumvent this problem by replacing the model for the geothermal storage by a so-called *analogous model* which is LTI.

The key idea for the construction of such an analogue is based on the observation that under the assumption of this paper our “original model” is already piecewise LTI. This is due to our assumption that the fluid velocity is constant \bar{v}_0 during (dis)charging when the pump is on, and zero during waiting when the pump is off. This leads to the following approximation of the original by an analogous model which is performed in two steps.

Approximation Step 1. For the analogous model we assume that contrary to the original model the fluid is also moving with constant velocity \bar{v}_0 during pump-off periods. During these waiting periods in the original model the fluid is at rest and only subject to the diffusive propagation of heat. In order to mimic that behavior of the resting fluid by a moving fluid we assume that the temperature Q^I at the PHX inlet is equal to the average temperature of the fluid in the PHX \bar{Q}^F . From a physical point of view we will preserve the average temperature of the fluid but a potential temperature gradient along the PHX is not preserved and replaced by an almost flat temperature distribution. It can be expected that the error induced by this “mixing” of the fluid temperature in the PHX is small after sufficiently long (dis)charging periods leading to saturation with an almost constant temperature along the PHX.

In the mathematical description by an initial boundary value problem for the heat equation (2.1), the above approximation leads to a modified boundary condition at the inlet. During waiting the homogeneous Neumann boundary condition in (2.4) is replaced by a non-local coupling condition such that the inlet boundary condition reads as

$$Q = \begin{cases} Q^I(t), & \text{pump on,} \\ \bar{Q}^F(t), & \text{pump off,} \end{cases} \quad (x, y) \in \partial \mathcal{D}^I.$$

That condition is termed ‘non-local’ since the inlet temperature is not only specified by a condition to the local temperature distribution at the inlet boundary $\partial \mathcal{D}^I$ but it depends on the whole spatial temperature distribution in the fluid domain \mathcal{D}^F . Semi-discretization of the above boundary condition using approximation (4.1) of the average fluid temperature

\bar{Q}^F formally leads to a modification of the input term $g(t)$ of the system of ODEs (3.1) given in (3.4). That input term now reads as

$$g(t) = \begin{cases} (Q^I(t), Q^G(t))^T, & \text{pump on,} \\ (C^F Y, Q^G(t))^T, & \text{pump off.} \end{cases} \quad (5.1)$$

Further, the non-zero entries B_{l1} of the input matrix B given in (3.3) are modified. They are now no longer time-dependent but given by the constant $B_{l1} = \frac{a^F}{h_x^2} + \frac{\bar{v}_0}{h_x}$ which was already used during pump-on periods.

Approximation Step 2. From (5.1) it can be seen that the input term g during pumping depends on the state vector Y via $C^F Y$ and can no longer be considered as exogenous. Formally, the term $C^F Y$ has to be included in AY which would lead to an additional contribution to the system matrix A given by $B_{\bullet 1} C^F$ where $B_{\bullet 1}$ denotes the first column of B . Thus, the system matrix again would be time-dependent and the system not LTI. For the application of model reduction methods we therefore perform a second approximation step and treat \bar{Q}^F as an exogenously given quantity (such as Q^I and Q^G). This leads to a tractable approach since the Lyapunov balanced truncation technique applied in the next section generates low-dimensional systems depending only on the system matrices A, B but not on the input term g . Further, from an algorithmic or implementation point of view this is not a problem since given the solution Y of (3.1) at time t , the average fluid temperature $\bar{Q}^F(t)$ can be computed as a linear combination of the entries of $Y(t)$.

In our companion paper [38, Sec. 6] we present results of numerical experiments indicating that apart from some small approximation errors in the PHX during waiting periods, in particular at the outlet, the other deviations are negligible. They also show that during the (dis)charging periods the errors decrease and vanish almost completely, i.e., in the long run there is no accumulation of errors.

6 Model Order Reduction

6.1 Problem

In the previous sections we have seen that the spatio-temporal temperature distribution describing the input-output behavior of the geothermal storage can be approximately computed by solving the system of ODEs (3.1) for the n -dimensional function $Y(t)$ resulting from semi-discretization of the heat equation (2.1). Aggregated characteristics can be obtained by linear combinations of the entries of Y in a post-processing step, see Sec. 4. In the following we will work with the approximation by an analogous system introduced in Sec. 5. Then the input-output behavior of the geothermal storage can be described by a LTI system, i.e., a pair of a linear autonomous differential and a linear algebraic equation which is well-known from linear system and control theory and of the form

$$\begin{aligned} \dot{Y}(t) &= AY(t) + Bg(t), \\ Z(t) &= CY(t). \end{aligned} \quad (6.1)$$

Here, $A \in \mathbb{R}^{n \times n}$, $B \in \mathbb{R}^{n \times m}$, $C \in \mathbb{R}^{n_o \times n}$ for $n, m, n_o \in \mathbb{N}$ are called *system*, *input*, *output matrix*, respectively. Further, $g : [0, T] \rightarrow \mathbb{R}^m$ is the *input* (or control), $Y : [0, T] \rightarrow \mathbb{R}^n$ the state and $Z : [0, T] \rightarrow \mathbb{R}^{n_o}$ is the *output*. Given some initial value $Y(0) = y_0$ the input-output

behavior, i.e., the mapping of the input g to the output Z is fully described by the triple of matrices (A, B, C) which is called *realization* of the above system.

For the analogous system A and B are constant matrices which are given in (3.2) and (3.3) for the case of constant velocity $v_0(t) = \bar{v}_0$, i.e., the pump is on. From Theorem 3.2 we know that A is stable. The input dimension is $m = 2$ while the dimension n of the state depends on the discretization of the spatial domain \mathcal{D} . The two entries of the input g are the temperatures at the inlet and of the underground at the bottom boundary. Thus g is piecewise continuous and bounded. The output Z contains the desired aggregated characteristics such as the average temperatures \bar{Q}^\dagger of the medium, the fluid, at the outlet or the bottom boundary. The associated row matrices C^\dagger of the approximation $\bar{Q}^\dagger(t) = C^\dagger Y(t)$ given in (4.4) form the n_o rows of the output matrix C . The output dimension n_o is the number of characteristics included in the problem and typically small while the state dimension n will be very large in order to obtain a reasonable accuracy for the semi-discretized solution of the heat equation (2.1).

For the above systems with high-dimensional state the simulation of the input-output behavior and the solution of optimal control problems suffer from the curse of dimensionality because of the computational complexity and storage requirements. This motivates us to apply model order reduction (MOR).

The general goal of MOR is to approximate the high-dimensional linear time-invariant system (6.1) given by the realization (A, B, C) by a low-dimensional reduced-order system

$$\begin{aligned}\tilde{Y}(t) &= \tilde{A}\tilde{Y}(t) + \tilde{B}g(t) \\ \tilde{Z}(t) &= \tilde{C}\tilde{Y}(t),\end{aligned}\tag{6.2}$$

i.e., a realization $(\tilde{A}, \tilde{B}, \tilde{C})$ where $\tilde{A} \in \mathbb{R}^{\ell \times \ell}$, $\tilde{B} \in \mathbb{R}^{\ell \times m}$, $\tilde{C} \in \mathbb{R}^{n_o \times \ell}$, $\tilde{Y} \in \mathbb{R}^\ell$, $\tilde{Z} \in \mathbb{R}^{n_o}$ and $\ell \ll n$ denotes the dimension of the reduced-order state. We notice that the input variable g is the same for systems (6.1) and (6.2). The reduced-order system should capture the most dominant dynamics of the original system in particular preserve the main physical system properties, e.g., stability. Further, it should provide a reasonable approximation of the original output Z by \tilde{Z} to given input g where the output error $Z - \tilde{Z}$ is measured using a suitable norm. In addition, the computation of the reduced-order system should be numerically stable and efficient.

Below we will derive a reduced-order model using Lyapunov balanced truncation. That method belongs to projection-based methods which are sketched next.

6.2 Projection-Based Methods

The underlying idea of projection-based methods is that the state dynamics can be well approximated by the dynamics of a projection of the n -dimensional state Y onto a suitable low-dimensional subspace of \mathbb{R}^n of dimension $\ell < n$. Then the aim is to describe the dynamics of the projection by a ℓ -dimensional system of ODEs. Prominent examples are the modal truncation and balanced truncation method, see Antouslas [2, Secs. 7, 9.2]. Here, the projection is found by applying a suitable linear state *transformation* $\bar{Y} = \mathcal{T}Y$ with some non-singular $n \times n$ -matrix \mathcal{T} which allows to define the projection by *truncation* of \bar{Y} , i.e., replacing the last $n - \ell$ entries by zero.

Transformation. The above mentioned transformation allows to derive the following alternative equivalent realization of the system (6.1) which is proven in Appendix B.1.

Lemma 6.1 *Let \mathcal{T} be a $n \times n$ constant non-singular transformation matrix. If we define the transformation $\bar{Y} = \mathcal{T}Y$, then the state and output equation in (6.1) become*

$$\begin{aligned}\dot{\bar{Y}}(t) &= \bar{A} \bar{Y}(t) + \bar{B}g(t), \\ Z(t) &= \bar{C} \bar{Y}(t).\end{aligned}\tag{6.3}$$

The realization of the system is given by $(\bar{A}, \bar{B}, \bar{C})$ where

$$\bar{A} = \mathcal{T}A\mathcal{T}^{-1}, \quad \bar{B} = \mathcal{T}B \quad \text{and} \quad \bar{C} = C\mathcal{T}^{-1}.$$

Truncation. After transforming the system we proceed to the truncation step. It is assumed that the transformation \mathcal{T} is such that the first ℓ entries of the transformed state \bar{Y} forming the ℓ -dimensional vector \bar{Y}_1 represent the “most dominant” states while the remaining $n - \ell$ entries which are collected in the $(n - \ell)$ -dimensional vector \bar{Y}_2 comprise the “less dominant” and “negligible” states. Based on this decomposition of \bar{Y} into \bar{Y}_1 and \bar{Y}_2 the following partition of system (6.3) into blocks is obtained

$$\begin{pmatrix} \dot{\bar{Y}}_1 \\ \dot{\bar{Y}}_2 \end{pmatrix} = \begin{pmatrix} \bar{A}_{11} & \bar{A}_{12} \\ \bar{A}_{21} & \bar{A}_{22} \end{pmatrix} \begin{pmatrix} \bar{Y}_1 \\ \bar{Y}_2 \end{pmatrix} + \begin{pmatrix} \bar{B}_1 \\ \bar{B}_2 \end{pmatrix} g(t), \quad Z = (\bar{C}_1 \ \bar{C}_2) \begin{pmatrix} \bar{Y}_1 \\ \bar{Y}_2 \end{pmatrix}.$$

The above block partition of the equivalent realization (6.3) is used to define the reduced-order system by assuming that the truncation of \bar{Y} to the first ℓ entries defines the desired projection. Then replacing the “negligible” states \bar{Y}_2 by zero and keeping only the first ℓ state equations for \bar{Y}_1 leads to the system

$$\dot{\bar{Y}}_1 = \bar{A}_{11}\bar{Y}_1 + \bar{B}_1g(t), \quad \bar{Z} = \bar{C}_1\bar{Y}_1.\tag{6.4}$$

Thus is the desired reduced-order system (6.2) is given by the realization $(\tilde{A}, \tilde{B}, \tilde{C}) = (\bar{A}_{11}, \bar{B}_1, \bar{C}_1)$ and approximates the output Z of the original system (6.1) by $\tilde{Z} = \bar{Z}$.

6.3 Lyapunov Balanced Truncation

6.3.1 Setting

The crucial question for the above introduced projection-based methods for MOR is the choice of a “suitable” transformation matrix \mathcal{T} which was left out and will be addressed in this subsection. The transformation should be such that the first entries of the transformed state \bar{Y} provide the largest contribution to the input-output behavior of the system. They carry the essential information for approximating the system output Z to a given input g with sufficiently high accuracy. On the other hand the last entries should deliver the smallest contribution to the input-output behavior and thus can be neglected.

Lyapunov balanced truncation uses ideas from control theory in particular the notion of controllability and observability which we sketch below. The basic idea is to define a transformation \mathcal{T} that “balances” the state in a way that the first ℓ entries of \bar{Y} are the states which are the easiest to observe and to reach. Then states which are simultaneously difficult to reach and to observe can be neglected and are truncated. That method appears

to be well-suited for the present problem of approximation input-output behavior of the geothermal storage. Balanced truncation MOR was first presented by Moore [29] who exploited results of Mullis and Roberts [30]. The preservation of stability was addressed by Pernebo and Silverman [32], error bounds derived by Enns [15] and Glover [17]

In the following we will always assume that the linear system (6.1) is stable, i.e., the system matrix A is stable. From Theorem 3.2 it is known that this is the case in the problem under consideration. This allows that the system dynamics is not only considered on finite time intervals $[0, T]$ but also on $[0, \infty)$.

Given the initial state $Y(0) = y_0$ and the control g , there exists a unique solution to the continuous-time dynamical system (6.1) given by

$$\begin{aligned} Y(t) &= \psi(t; y_0, u) := e^{At}y_0 + \int_0^t e^{A(t-s)}Bg(s)ds, \\ Z(t) &= CY(t) = Ce^{At}y_0 + \int_0^t Ce^{A(t-s)}Bg(s)ds. \end{aligned} \quad (6.5)$$

Note that the first term in the above state equation is $\psi(t; y_0, 0)$ representing the response to an initial condition y_0 and to a zero input while the second term is $\psi(t; 0, g)$ and represents the response to a zero initial state and input g .

6.3.2 Controllability and Observability

We now introduce some concepts from linear system theory which will play a crucial role in the derivation of the balanced truncation method. Let us denote by $\mathcal{L}_2(0, t)$ the space of square integrable functions on $[0, t]$ with the induced norm $\|f\|_{\mathcal{L}_2(0, t)} = (\int_0^t \|f(s)\|_2^2 ds)^{1/2}$. We write $\mathcal{L}_2(0, \infty)$ for functions on $[0, \infty)$.

Definition 6.2 (Controllability)

1. Let the linear system (6.1) be given. A state $y \in \mathbb{R}^n$ is said to be **controllable** from zero initial state $y_0 = 0$ if there exist a finite time t^* and an input $g \in \mathcal{L}_2(0, t^*)$ such that the solution given in (6.5) satisfies $Y(t^*) = \psi(t^*, 0, g) = y$.
2. The **controllable** or reachable **subspace** \mathcal{Y}_C is the set of states that can be obtained from zero initial state and a given input $g \in \mathcal{L}_2(0, t^*)$.
3. The linear system (6.1) is said to be (completely) controllable if $\mathcal{Y}_C = \mathbb{R}^n$.

We note that for LTI systems the controllable subspace \mathcal{Y}_C is invariant w.r.t. the choice of the initial state y_0 . This allows the above restriction to controllability from zero initial state.

Definition 6.3 (Observability)

1. Let the linear system (6.1) be given and let $g = 0$. A state $y \in \mathbb{R}^n$ is said to be **unobservable** if the output $Z(t) = C\psi(t, y, 0) = 0$ for all $t \geq 0$, i.e., for all $t \geq 0$ the output $Z(t)$ of the system to initial state $Y(0) = y$ is indistinguishable from the output to zero initial state. Otherwise the state y is called **observable**.
2. The **observable subspace** \mathcal{Y}_O is the set all observable states.
3. System (6.1) is said to be (completely) observable if $y = 0$ is the only unobservable state.

Remark 6.4 Let Y_1, Y_2 and Z_1, Z_2 denote state and output of system (6.1) to initial states y_1, y_2 and the same input g . If system (6.1) is observable then the equality of outputs $Z_1(t) = Z_2(t)$ for all $t \geq 0$ implies that $y_1 = y_2$. Otherwise it holds $y_1 \neq y_2$. This can easily be seen from the consideration for $Y = Y_1 - Y_2$ and $Z = Z_1 - Z_2$ which are the state and the output to initial state $y = 0$ and input $g = 0$.

The input-output behavior of system (6.1) can be quantified by the following measures of the “degree of controllability and observability”. They are based on the (squared) $\mathcal{L}_2(0, \infty)$ -norms of the input and output functions which in the literature are often called “input and output energy”.

Definition 6.5 (Controllability and Observability Function)

1. The controllability function $\mathcal{E}_C : \mathcal{Y}_C \rightarrow [0, \infty)$ is given for $y \in \mathcal{Y}_C$ by

$$\mathcal{E}_C(y) = \min_{\substack{g \in \mathcal{L}_2(0, \infty) \\ Y(0)=0, Y(\infty)=y}} \|g\|_{\mathcal{L}_2(0, \infty)}^2 = \min_{\substack{g \in \mathcal{L}_2(0, \infty) \\ Y(0)=0, Y(\infty)=y}} \int_0^\infty \|g(t)\|_2^2 dt. \quad (6.6)$$

2. The observability function $\mathcal{E}_O : \mathbb{R}^n \rightarrow [0, \infty)$ is given for $y \in \mathbb{R}^n$ by

$$\mathcal{E}_O(y) = \|Z\|_{\mathcal{L}_2(0, \infty)}^2 = \int_0^\infty \|Z(t)\|_2^2 dt, \quad Y(0) = y, g(t) = 0 \quad \text{for all } t \geq 0. \quad (6.7)$$

The controllability function $\mathcal{E}_C(y)$ is the smallest input energy required to reach the state $y \in \mathcal{Y}_C$ from zero initial state in infinite time. In view of the definition of a controllable state y given in Def. 6.2 the minimization is w.r.t. both the input function and the terminal time t^* . For more details see Antouslas [2, Lemma 4.29]. The observability function $\mathcal{E}_O(y)$ is obtained as the limit of the output energy on a finite time interval $[0, T]$ for $T \rightarrow \infty$. Since the output energy increases in T we can consider $\mathcal{E}_O(y)$ as the maximum output energy produced by the system when it is released from initial state y for zero input.

The above quantities allow the following interpretation. States which are difficult to reach are characterized by large values of the controllability function $\mathcal{E}_C(y)$. They require large input energy to reach them. On the other hand, for large values of the observability function $\mathcal{E}_O(y)$ the state y is easy to observe whereas small values of $\mathcal{E}_O(y)$ indicate that state y is difficult to observe since it produces only small output energy. Note, that unobservable states don't produce output energy at all and it holds $\mathcal{E}_O(y) = 0$ for $y \notin \mathcal{Y}_O$.

6.3.3 Gramians

Below we will see that the controllability and observability function can be expressed in terms of the following matrices, see Antouslas [2, Sec. 4.3]

Definition 6.6 (Controllability and Observability Gramian)

Consider a stable linear system (6.1). The matrices defined by

$$\mathcal{G}_C = \int_0^\infty e^{At} B B^\top e^{A^\top t} dt,$$

$$\mathcal{G}_O = \int_0^\infty e^{A^\top t} C^\top C e^{At} dt.$$

are called (infinite) **controllability and observability Gramians**, respectively.

The Gramians enjoy the following properties.

Lemma 6.7 *The Gramians \mathcal{G}_C and \mathcal{G}_O are symmetric, positive semi-definite matrices. If the linear system (6.1) is stable, controllable and observable then the Gramians are strictly positive definite.*

Proof. The first two properties follow directly from the definition of the Gramians. The third property is proven in Theorems 2.2 and 3.2 of Davis et al. [14].

Theorem 6.8 *Let the linear system (6.1) be a stable, controllable and observable. Then the controllability and observability function defined in (6.6) and (6.7) are given by*

$$\begin{aligned}\mathcal{E}_C(y) &= y^\top \mathcal{G}_C^{-1} y \quad \text{for } y \in \mathcal{V}_C, \\ \mathcal{E}_O(y) &= y^\top \mathcal{G}_O y \quad \text{for } y \in \mathbb{R}^n.\end{aligned}\tag{6.8}$$

The proof of the above theorem is given in Appendix B.2. The above relations show that states y in the span of the eigenvectors corresponding to small (large) eigenvalues of \mathcal{G}_C lead to large (small) values of $\mathcal{E}_C(y)$. Thus such states require a high (small) input energy and are difficult (easy) to reach. On the other hand, states y in the span of the eigenvectors corresponding to small eigenvalues of \mathcal{G}_O produce only small output energy $\mathcal{E}_O(y)$ and are difficult to observe.

The Gramians are therefore efficient tools to quantify the degree of controllability and observability of a given state. Further the eigenvectors of \mathcal{G}_C and \mathcal{G}_O span the controllable and observable subspaces, respectively.

6.3.4 Computation of Gramians

The computation of the Gramians according to the Def. 6.6 is quite cumbersome. A computationally feasible method is based on the following theorem stating that the Gramians satisfy some linear matrix equations.

Theorem 6.9 *Let the linear system (6.1) be a stable. Then the controllability Gramian \mathcal{G}_C and observability Gramian \mathcal{G}_O satisfy the algebraic Lyapunov equations*

$$\begin{aligned}A\mathcal{G}_C + \mathcal{G}_CA^\top &= -BB^\top, \\ \mathcal{G}_OA + A^\top\mathcal{G}_O &= -C^\top C.\end{aligned}$$

The proof can be found in Antouglas [2, Proposition 4.27] and is also provided in Appendix B.3.

Remark 6.10 For solving the above Lyapunov matrix equation usually numerical methods have to be applied. Such methods have been addressed in a large body of literature. For a low-dimensional and dense matrix A , the Lyapunov equations can be solved using Hammarling method [22, 24], for medium- to large-scale Lyapunov equations, a sign function method [9, 12] can be used, in the case of large and sparse matrix A , projection-type methods such as \mathcal{H} -matrices based methods [21], Krylov subspace methods [25, 35] and alternating direction implicit (ADI) method [7, 6, 31] are more appropriate for solving Lyapunov equations.

6.3.5 Balancing

We now come back to the construction of a “suitable” transformation matrix \mathcal{T} which should be such that the first entries of the transformed state $\bar{Y} = \mathcal{T}Y$ provide the largest contribution to the input-output behavior of the system. The idea of Lyapunov balanced truncation is to use a transformation \mathcal{T} that “balances” the state such that the first entries of \bar{Y} are simultaneously easy to reach and easy to observe. This allows to truncate the remaining states which are difficult to reach and difficult to observe.

We recall the interpretation of the Gramians after Theorem 6.8. States that are easy to reach, i.e., those that require a small amount of input energy to reach, are found in the span of the eigenvectors of the controllability Gramian \mathcal{G}_C corresponding to large eigenvalues. Further, states that are easy to observe, i.e., those that produce large amounts of output energy, lie in the span of eigenvectors of the observability Gramian \mathcal{G}_O corresponding to large eigenvalues as well. However, in an arbitrary coordinate system a state y that is easy to reach might be difficult to reach. On the other hand, there might exist a different state y' that is difficult to reach but easy to observe. Then it is hard to decide which of the two states y and y' is more important for the input-output behavior of the system.

This observation suggests to transform the coordinate system of the state space using a transformation matrix \mathcal{T} in which states that are easy to reach are simultaneously easy to observe and vice versa. This is the case if the transformed Gramians coincide. Below we give a transformation for which the two Gramians are even diagonal.

We recall Lemma 6.1 which describes the transformation of the realization (A, B, C) of system (6.1) to the realization $(\bar{A}, \bar{B}, \bar{C})$ of the transformed system (6.3). The following lemma describes the transformation of the corresponding Gramians.

Lemma 6.11 *Let \mathcal{T} be a $n \times n$ non-singular transformation matrix defining the transformed system (6.3) for the transformed state $\bar{Y} = \mathcal{T}Y$.*

For the transformed Gramians $\bar{\mathcal{G}}_C$ and $\bar{\mathcal{G}}_O$ of that system it holds

$$\bar{\mathcal{G}}_C = \mathcal{T} \mathcal{G}_C \mathcal{T}^\top, \quad \bar{\mathcal{G}}_O = \mathcal{T}^{-\top} \mathcal{G}_O \mathcal{T}^{-1} \quad \text{and} \quad \bar{\mathcal{G}}_C \bar{\mathcal{G}}_O = \mathcal{T} \mathcal{G}_C \mathcal{G}_O \mathcal{T}^{-1}.$$

The proof of Lemma 6.11 can be found in Appendix B.4. The last relation of the above lemma shows that the product $\bar{\mathcal{G}}_C \bar{\mathcal{G}}_O$ results from a similarity transformation of the product $\mathcal{G}_C \mathcal{G}_O$. Thus the eigenvalues of the product of the two Gramians are preserved under transformations of the coordinate system and can be considered as system invariants. They can be expressed as squares of the Hankel singular values of the system.

Definition 6.12 (Hankel Singular Values) *The Hankel singular values are the square roots of the eigenvalues of the product of the controllability and observability Gramian*

$$\sigma_i = \sqrt{\lambda_i(\mathcal{G}_C \mathcal{G}_O)}, \quad i = 1, \dots, n.$$

Here $\lambda_i(G)$ denotes the i -th eigenvalue of the matrix G , ordered as $\lambda_1 \geq \lambda_2 \geq \dots \lambda_n \geq 0$.

For linear systems (6.1) which are controllable, observable and stable it is known that the Hankel singular values are strictly positive, see Antoulas [2, Lemma 5.8].

The next theorem presents the main result of Lyapunov balanced truncation and gives the transformation matrix \mathcal{T} that balances the system such that the two Gramians are equal and diagonal.

Theorem 6.13 (Balancing Transformation)

Let the linear system (6.1) be stable, controllable and observable. Further, let

$\mathcal{G}_C = UU^\top$ be the Cholesky decomposition of the controllability Gramian
where U is an upper triangular matrix,

$U^\top \mathcal{G}_O U = K \Sigma^2 K^\top$ be the eigenvalue decomposition of $U^\top \mathcal{G}_O U$ such that

$\Sigma = \text{diag}(\sigma_1, \dots, \sigma_n)$ is the diagonal matrix of Hankel singular values from Def. 6.12.
Then for the transformation matrix

$$\mathcal{T} = \Sigma^{\frac{1}{2}} K^\top U^{-1} \quad (6.9)$$

the transformed system (6.3) is balanced and the controllability $\bar{\mathcal{G}}_C$ and observability $\bar{\mathcal{G}}_O$ Gramians are given by

$$\bar{\mathcal{G}}_C = \bar{\mathcal{G}}_O = \Sigma$$

i.e., they are diagonal and equal to a diagonal matrix containing the Hankel singular values as diagonal entries

The proof of Theorem 6.13 can be found in Appendix B.5.

The above approach may be numerically inefficient and ill-conditioned. The reason is that for large-scale systems the Gramians $\mathcal{G}_C, \mathcal{G}_O$ often have a numerically low rank compared to the dimension n . This is due to the fast decay of the eigenvalues of the Gramians and also of the Hankel singular values. Then the computation of inverse matrices such as U^{-1} should be avoided from an numerical point of view. In the literature there are several suggestions of alternative approaches which are identical in theory but yield algorithms with different numerical properties, see Antoulas [2, Sec. 7.4] and the references therein. One of them is given in the next theorem.

Theorem 6.14 (Square Root Algorithm, Antoulas [2], Sec. 7.4)

Let the assumptions of Theorem 6.13 be fulfilled. Further, let

$\mathcal{G}_C = UU^\top$ be the Cholesky decomposition of the controllability Gramian,

$\mathcal{G}_O = LL^\top$ be the Cholesky decomposition of the observability Gramian,

where U is an upper and L a lower triangular matrix,

$U^\top L = W \Sigma V^\top$ be the singular value decomposition of $U^\top L$ with the
orthogonal matrices W and V .

Then the transformation matrix \mathcal{T} given in (6.9) and its inverse can be represented as

$$\mathcal{T} = \Sigma^{-1/2} V^\top L^\top \quad \text{and} \quad \mathcal{T}^{-1} = U W \Sigma^{-1/2}. \quad (6.10)$$

Note that the computation of \mathcal{T} according to (6.10) does not require the inversion of the full matrix U as in (6.9).

6.3.6 Truncation

The final step of the balanced truncation MOR is the truncation of the balanced system as it is explained in Subsec. 6.2. Then the truncated balanced system as in (6.4) is the desired reduced-order system (6.2). It is also balanced and Antoulas [2] shows in Theorem 7.9 that for $\sigma_\ell > \sigma_{\ell+1}$ the reduced-order system is again stable, controllable and observable.

6.3.7 Algorithm

Let the linear LTI system (6.1) with the realization (A, B, C) be stable, controllable and observable. Then, the balanced truncation procedure can be summarized in the following algorithm.

Algorithm 6.15 (Lyapunov Balanced Truncation)

- 1) Compute the Gramians \mathcal{G}_C and \mathcal{G}_O by solving the Lyapunov equations
 $A\mathcal{G}_C + \mathcal{G}_CA^\top = -BB^\top$ and $\mathcal{G}_OA + A^\top\mathcal{G}_O = -C^\top C$.
- 2) Compute the Cholesky decomposition of the Gramians $\mathcal{G}_C = UU^\top$ and $\mathcal{G}_O = LL^\top$
 where U is an upper and L is a lower triangular matrix.
- 3) Compute the singular value decomposition
 $U^\top L = W\Sigma V^\top$ with $\Sigma = \text{diag}(\sigma_1, \dots, \sigma_n)$ and $\sigma_1 \geq \sigma_2 \geq \dots \geq \sigma_n > 0$.
- 4) Construct the transformation matrices $\mathcal{T} = \Sigma^{-1/2}V^\top L^\top$ and $\mathcal{T}^{-1} = UW\Sigma^{-1/2}$.
- 5) Transforming the state to $\bar{Y} = \mathcal{T}Y$ leads to the balanced system defined by the matrices

$$(\bar{A}, \bar{B}, \bar{C}) = (\mathcal{T}A\mathcal{T}^{-1}, \mathcal{T}B, C\mathcal{T}^{-1}) = \left(\begin{pmatrix} \bar{A}_{11} & \bar{A}_{12} \\ \bar{A}_{21} & \bar{A}_{22} \end{pmatrix}, \begin{pmatrix} \bar{B}_1 \\ \bar{B}_2 \end{pmatrix}, (\bar{C}_1 \ \bar{C}_2) \right).$$

- 6) Truncate the transformed state $\bar{Y} = \mathcal{T}Y$ keeping the first ℓ entries and choose

$$(\tilde{A}, \tilde{B}, \tilde{C}) = (\bar{A}_{11}, \bar{A}_1, \bar{C}_1), \quad \tilde{A} \in \mathbb{R}^{\ell \times \ell}, \quad \tilde{B} \in \mathbb{R}^{\ell \times m}, \quad \tilde{C} \in \mathbb{R}^{n_o \times \ell}.$$

Remark 6.16

1. From an implementation point of view in the above algorithm the truncation in step 6 can be moved to step 4 which allows the construction of the reduced-order system without forming the high-dimensional balanced system in step 5. This leads to the following modification of Algorithm 6.15.

- 4*) Define the diagonal matrix $\Sigma_\ell = \text{diag}(\sigma_1, \dots, \sigma_\ell)$ formed by the ℓ largest Hankel singular values and the $n \times \ell$ matrices W_ℓ, V_ℓ formed by the first ℓ columns of W, V , respectively.

Construct new transformation matrices with the $\ell \times n$ matrix $\mathcal{T}_\ell^+ = \Sigma_\ell^{-1/2}V_\ell^\top L^\top$ and the $n \times \ell$ matrix $\mathcal{T}_\ell^- = UW_\ell\Sigma_\ell^{-1/2}$.

Note that $\mathcal{T}^+\mathcal{T}^- = I_\ell$ is the identity matrix of dimension ℓ .

- 5*) omitted

- 6*) The reduced-order system is obtained directly by

$$(\tilde{A}, \tilde{B}, \tilde{C}) = (\mathcal{T}^+A\mathcal{T}^-, \mathcal{T}^+B, C\mathcal{T}^-).$$

That modification is also interesting from an computational point of view since it requires not the full but only a partial singular value decomposition of $U^\top L$ in step 3.

2. The above modification is also useful for linear systems which are not (fully) observable or controllable as it is often the case if system (6.1) results from the semi-discretization of PDEs. We also observe this for the system derived in above in (3.1). Then the Gramians $\mathcal{G}_C, \mathcal{G}_O$ and also the product $\mathcal{G}_C \mathcal{G}_O$ might be singular and there are zero Hankel singular values such that we have $\sigma_1 \geq \dots \geq \sigma_{n_0} > 0 = \sigma_{n_0+1} = \dots = \sigma_n$ for some $n_0 < n$. In that case the transformation matrix \mathcal{T} and its inverse \mathcal{T}^{-1} are not defined and the above algorithm breaks down. However \mathcal{T}^+ and \mathcal{T}^- are well-defined for any $\ell \leq n_0$ and formally the above described modification works well.

A theoretical justification of that approach is given in Tombs and Postlethwaite [39, Thm. 2.2]. The authors show that for $\ell = n_0$ the reduced-order system is stable, fully controllable and observable and has the same transfer function as the original system, i.e. there is no change of the input-output behavior. This allows to fit a stable but not necessarily fully observable and controllable system into the above framework from the beginning of this section. In a preprocessing step balanced truncation is formally applied to obtain a reduced-order system of dimension $\ell = n_0$. The latter system is stable, controllable and observable and can be further reduced applying the standard methods to obtain an approximation of the input-output behavior.

6.3.8 Error Bounds

One of the advantages of Lyapunov balanced truncation is that there exist error estimates which can be given in terms of the discarded Hankel singular values. They allow to select the dimension ℓ of the reduced-order system such that a prescribed accuracy of the output approximation is guaranteed. In the literature these error estimates are given for the transfer functions of the original and the reduced-order system from which one can derive the estimates given below for the error measured in the $\mathcal{L}_2(0, t)$ -norm. The following theorem is proven in Enns [15] and Glover [17].

Theorem 6.17 *Let the linear system (6.1) be a stable, controllable and observable with zero initial value, i.e. $Y(0) = 0$. Further, let Hankel singular values be pairwise distinct with $\sigma_1 > \dots > \sigma_n > 0$. Then it holds for all $t \geq 0$*

$$\|Z - \tilde{Z}\|_{\mathcal{L}_2(0, t)} \leq 2 \sum_{i=\ell+1}^n \sigma_i \|g\|_{\mathcal{L}_2(0, t)}. \quad (6.11)$$

The error bound given in (6.11) depends on the reduced order ℓ only via the sum of discarded Hankel singular values for which we have

$$\sum_{i=\ell+1}^n \sigma_i = \text{tr}(\Sigma_2) = \text{tr}(\Sigma) - \text{tr}(\Sigma_1),$$

where $\Sigma_1 = \text{diag}(\sigma_1, \dots, \sigma_\ell)$ and $\Sigma_2 = \text{diag}(\sigma_{\ell+1}, \dots, \sigma_n)$. According to Theorem 6.13 we have that $\bar{\mathcal{G}}_C = \bar{\mathcal{G}}_O = \Sigma$, i.e., the controllability and observability Gramians of the balanced system are equal to the diagonal matrix Σ . Further, the two Gramians of the reduced-order system are also equal and given by the diagonal matrix Σ_1 . We recall Theorem 6.8 which states that the output energy contained in the output Z when the system is released from initial state y for zero input is given by $\mathcal{E}_O(y) = \|Z\|_{\mathcal{L}_2(0, \infty)}^2 = y^\top \mathcal{G}_O y$, see (6.7) and (6.8). Given the balanced realization of the original system (6.1) the output energy related to the

initial state $Y(0) = \mathbb{1}_n$, i.e., the vector with all entries equal one, is $\mathcal{E}_O(\mathbb{1}_n) = \mathbb{1}_n^\top \Sigma \mathbb{1}_n = \text{tr}(\Sigma)$. Analogously, for the reduced-order system the output energy related to the initial state $\tilde{Y}(0) = \mathbb{1}_\ell$ obtained by truncation of $\mathbb{1}_n$ to the first ℓ entries is given by $\mathcal{E}_O(\mathbb{1}_\ell) = \|\tilde{Z}\|_{\mathcal{L}_2(0,\infty)}^2 = \text{tr}(\Sigma_1)$. Thus the sum of discarded Hankel singular values which is $\text{tr}(\Sigma) - \text{tr}(\Sigma_1)$ can be interpreted as the loss of output energy due to truncation if the balanced system starts with an initial “excitation” where all (balanced) states are equal one and no forcing is applied, i.e., the input g is zero.

Obviously, the above sum is decreasing in ℓ and reaches zero for $\ell = n$. This motivates the introduction of the following relative selection criterion

$$\mathcal{S}(\ell) = \frac{\text{tr}(\Sigma_1)}{\text{tr}(\Sigma)}, \quad \text{for } \ell = 1, \dots, n,$$

with values in $(0, 1]$. It is increasing in ℓ reaching $\mathcal{S}(\ell) = 1$ for $\ell = n$. $\mathcal{S}(\ell)$ can be used as a measure of the proportion of the output energy which can be captured by a reduced-order system of dimension ℓ . The selection of an appropriate dimension ℓ can be based on a prescribed threshold level $\alpha \in (0, 1]$ for that proportion for which the minimal reduced order reaching that level is defined by

$$\ell_\alpha = \min\{\ell : \mathcal{S}(\ell) \geq \alpha\}. \quad (6.12)$$

Remark 6.18

1. Since the Hankel singular values only depend on the original model (6.1) the error bound in (6.11) can be computed a priori. Given the input g this allows to control the approximation error by the selection of the reduced order ℓ .
2. The reverse triangular inequality yields $\|Z - \tilde{Z}\|_{\mathcal{L}_2(0,t)} \geq \left| \|Z\|_{\mathcal{L}_2(0,t)} - \|\tilde{Z}\|_{\mathcal{L}_2(0,t)} \right|$. Hence, the error bound in (6.11) also applies to the difference of the \mathcal{L}_2 -norms of the output Z and its approximation \tilde{Z} .
3. The error bound can be generalized to systems with Hankel singular values with multiplicity larger than one. In that case they only need to be counted once, leading to tighter bounds, see Glover [17].
4. The assumption of a zero initial state is quite restrictive and usually not fulfilled in applications. We refer to Beattie et al. [5], Daraghmeh et al. [13], Heinkenschloss et al. [23] and Schröder and Voigt [34] where the authors study the general case of linear systems with non-zero initial conditions and derive error bounds with extra terms accounting for the initial condition.
5. The linear systems considered in the present paper are obtained by semi-discretization of the heat equation (2.1) with the associated boundary and initial conditions. The initial value $Y(0) = y_0 \in \mathbb{R}^n$ represents the initial temperatures $Q(0, \cdot, \cdot)$ at the corresponding grid points. In general we have $y_0 \neq 0_n$. However, for the case of an homogeneous initial temperature distribution with $Q(0, x, y) = Q_0$ for all $(x, y) \in \mathcal{D}$ and some constant Q_0 one can derive an equivalent linear system with zero initial value. That case is considered in our numerical experiments in Sec. 7.

The idea is to shift the temperature scale by Q_0 and describe the temperature distribution by $\hat{Q}(t, x, y) = Q(t, x, y) - Q_0$. Then the initial condition reads as $\hat{Q}(0, x, y) = 0$. Thanks to linearity of the heat equation (2.1) and the boundary conditions \hat{Q} also satisfies the heat equation together with the boundary conditions if the inlet and ground temperature appearing in the Dirichlet and Robin condition are shifted accordingly, i.e., Q^I and Q^G are replaced by $Q^I - Q_0$ and $Q^G - Q_0$. Semi-discretization of the modified heat equation generates a linear system (6.1) with zero initial condition $Y(0) = 0_n$ for which we can apply the error estimate given in (6.11). The aggregated characteristics of the temperature distribution corresponding to the model with constant but non-zero initial temperature Q_0 and forming the system output Z can easily be derived from the output of the modified system. In a post-processing step the inverse shift of the temperature scale is applied where Q_0 is added to all temperatures.

7 Numerical Results

In this section we present results of numerical experiments on model order reduction for the system of ODEs (3.1) resulting from semi-discretization of the heat equation (2.1) which models the spatio-temporal temperature distribution of a geothermal storage. For describing the input-output behavior of that storage we use the aggregated characteristics of the spatial temperature distribution introduced in Sec. 4. Further we work with the approximation of (3.1) by an analogous system as explained in Sec. 5. Recall, that here it is assumed that the pump is always on and during the waiting periods the inlet temperature Q^I is set to be the average temperature \bar{Q}^F in the PHX fluid.

We present approximations of the aggregated characteristics obtained from reduced-order models together with error estimates provided in Theorem 6.17 for systems with zero initial conditions. Here we apply the approach sketched in Remark 6.18, item 5, where in a preprocessing step we first shift the temperature scale by the constant initial temperature Q_0 to obtain a linear system (6.1) with zero initial value for which we can compute the error bounds. Then in a postprocessing step the inverse scale shift is applied.

The experiments are based on Algorithm 6.15 and are performed for the cases of one and three PHXs. The model with three PHXs is more realistic and shows more structure of the spatial temperature distribution in the storage whereas for one PHX that distribution is less heterogeneous.

After explaining the experimental settings in Subsec. 7.1 we start in Subsec. 7.2 with an experiment where the system output consists of only one variable which is the average temperature \bar{Q}^M in the storage medium. For that case we restrict ourselves to charging and discharging the storage without intermediate waiting periods. Note that the analogous system requires during the waiting periods the knowledge of the average PHX temperature which in this experiment is not included in the output variables.

In order to allow to work with waiting periods we add in Subsec. 7.3 a second output variable which is the average PHX temperature \bar{Q}^F . Then we add a third output variable which is in Subsec. 7.4 the average temperature at the outlet \bar{Q}^O whereas in Subsec. 7.5 the average temperature at the bottom \bar{Q}^B of the storage is used as third output variable. The outlet temperature \bar{Q}^O is interesting for the management of heating systems equipped with a geothermal storage while \bar{Q}^B allows to quantify the transfer of thermal energy to the environment at the bottom boundary of the geothermal storage. Finally, Subsec. 7.6

presents results for a model where the output contains all of the four above mentioned quantities.

7.1 Experimental Settings

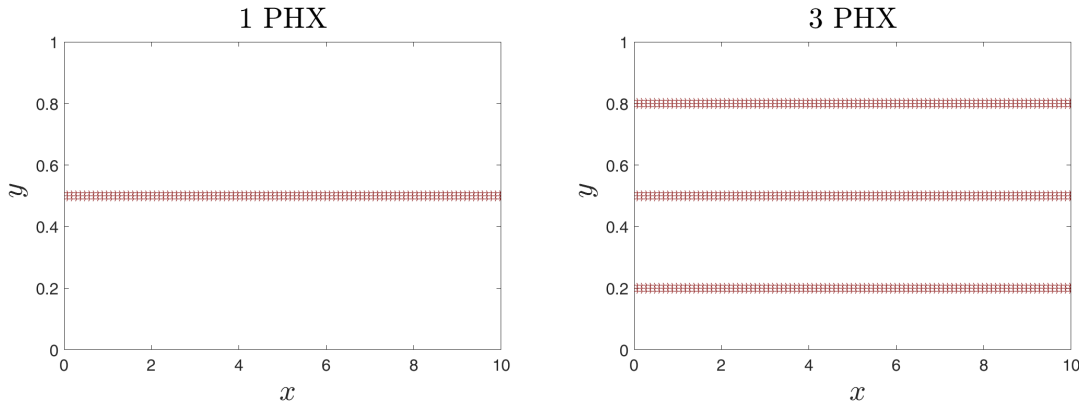


Fig. 7.1 Computational domain with horizontal straight PHXs. Left: one PHX . Right: three PHXs.

For our numerical examples we use the model and discretization parameters taken from our companion paper [38] and given in Table 7.1. The storage is charged and discharged either by a single PHX or by three PHXs filled with a moving fluid, see Fig. 7.1. Thermal energy is stored by raising the temperature of the storage medium. We recall the open architecture of the storage which is only insulated at the top and the side but not at the bottom. This leads to an additional heat transfer to the underground for which we assume a constant temperature of $Q^G(t) = 15^\circ\text{C}$. In all experiments we start with a homogeneous initial temperature distribution with the constant temperature $Q_0 = 10^\circ\text{C}$. The fluid is assumed to be water while the storage medium is dry soil. During charging a pump moves the fluid with constant velocity \bar{v}_0 arriving with constant temperature $Q^I(t) = Q_C^I = 40^\circ\text{C}$ at the inlet. This temperature is higher than in the vicinity of the PHXs, thus induces a heat flux into the storage medium. During discharging the inlet temperature is $Q^I(t) = Q_D^I = 5^\circ\text{C}$ leading to a cooling of the storage. At the outlet we impose a vanishing diffusive heat flux, i.e. during pumping there is only a convective heat flux. We also consider waiting periods where the pump is off. This helps to mitigate saturation effects in the vicinity of the PHXs which reduce the injection and extraction efficiency. During that waiting periods the injected heat (cold) can propagate to other regions of the storage. Without convection of the PHX fluid we have only diffusive propagation of heat in the storage and the transfer over the bottom boundary.

For the chosen discretization parameters the dimension of the state equation (6.1) resulting from the space-discretization of the heat equation is $n = 10201$. The output matrix C depends on the number of output variables and changes in the various experiments.

7.2 One Aggregated Characteristic: \bar{Q}^M

In this example we consider a model with only a single output variable $Z_1 = \bar{Q}^M$, the average temperature of the medium. Then the system output does not contain the average fluid

Parameters		Values	Units
Geometry			
width	l_x	10	m
height	l_y	1	m
depth	l_z	1	m
diameter of PHXs	d_P	0.02	m
number of PHXs	n_P	1 and 3	
Material			
<i>medium (dry soil)</i>			
mass density	ρ^M	2000	kg/m^3
specific heat capacity	c_p^M	800	$J/kg K$
thermal conductivity	κ^M	1.59	$W/m K$
thermal diffusivity	$\kappa^M (\rho^M c_p^M)^{-1}$	9.9375×10^{-7}	m^2/s
<i>fluid (water)</i>			
mass density	ρ^F	998	kg/m^3
specific heat capacity	c_p^F	4182	$J/kg K$
thermal conductivity	κ^F	0.60	$W/m K$
thermal diffusivity	$\kappa^F (\rho^F c_p^F)^{-1}$	1.4376×10^{-7}	m^2/s
velocity during pumping	\bar{v}_0	10^{-2}	m/s
heat transfer coeff. to underground	λ^G	10	$W/(m^2 K)$
initial temperature	Q_0	10	$^\circ C$
inlet temperature: charging	Q_C^I	40	$^\circ C$
discharging	Q_D^I	5	$^\circ C$
underground temperature	Q^G	15	$^\circ C$
Discretization			
step size	h_x	0.1	m
step size	h_y	0.01	m
time step	τ	1	s
time horizon	T	72	h

Table 7.1 Model and discretization parameters.

temperature \bar{Q}^F which serves in the analogous system as inlet temperature during waiting periods. Therefore we consider only charging and discharging periods without intermediate waiting periods. For horizon time $T = 72$ hours we divide the interval $[0, T]$ into a charging period $I_C = [0, T/2]$ followed by a discharging period $I_D = (T/2, T]$. The input function $g : [0, T] \rightarrow \mathbb{R}^2$ is defined as

$$g(t) = (Q^I(t), Q^G(t))^T \quad \text{with} \quad Q^I(t) = \begin{cases} Q_C^I = 40^\circ C & \text{for } t \in I_C \text{ (charging),} \\ Q_D^I = 5^\circ C & \text{for } t \in I_D \text{ (discharging),} \end{cases}$$

with the piece-wise constant inlet temperature $Q^I(t)$ and the constant underground temperature $Q^G(t) = 15^\circ C$. The output matrix in this case is given by $C = C^M$ which is given in our companion paper [38, Sec. 4].

In Fig. 7.2, the left panel shows first 50 largest Hankel singular values associated to the most observable and most reachable states whereas in the right panel we plot the selection criterion against the reduced order ℓ (red for 1 PHX and blue for 3 PHXs). For the first 50 singular values we observe for both models that they are all distinct and decrease fast by

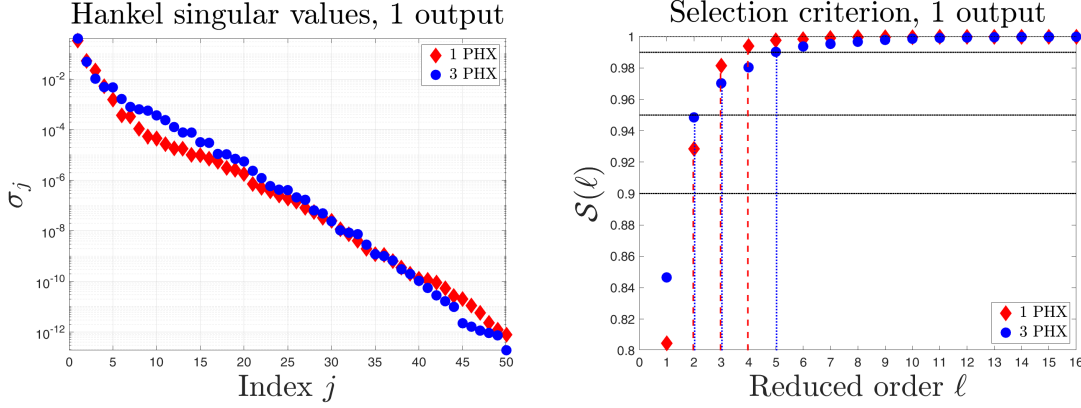


Fig. 7.2 Model with one output $Z = \overline{Q}^M$:

Left: first 50 largest Hankel singular values, Right: selection criterion.

12 orders of magnitude. The first 20 singular values decrease faster for the model with one PHX than for the 3 PHX model.

Output	α	90%	95%	99%
$Z = \overline{Q}^M$		2/2	3/3	4/5
$Z = (\overline{Q}^M, \overline{Q}^F)^\top$		4/4	5/6	11/11
$Z = (\overline{Q}^M, \overline{Q}^F, \overline{Q}^B)^\top$		5/6	7/8	12/13
$Z = (\overline{Q}^M, \overline{Q}^F, \overline{Q}^O)^\top$		8/8	10/9	15/14
$Z = (\overline{Q}^M, \overline{Q}^F, \overline{Q}^O, \overline{Q}^B)^\top$		9/9	11/11	17/16

Table 7.2 Minimal reduced orders $\ell_\alpha = \min\{\ell : \mathcal{S}(\ell) \geq \alpha\}$, 1 PHX / 3 PHXs.

We recall that the selection criterion $\mathcal{S}(\ell)$ provides an estimate of the proportion of output energy of the original system that can be captured by the reduced-order system of dimension ℓ . In the right panel of Fig. 7.2 we draw vertical red dashed (one PHX) and blue dotted lines (three PHX) to indicate the reduced orders ℓ for which the selection criterion $\mathcal{S}(\ell)$ exceeds the threshold values $\alpha = 90\%, 95\%, 99\%$ for the first time, respectively. This allows to determine graphically the associated minimal reduced orders $\ell_\alpha = \min\{\ell : \mathcal{S}(\ell) \geq \alpha\}$ which have been introduced in (6.12). The resulting values are also given in Table 7.2. It can be seen that already with $\ell_{0.9} = 2$ states the reduced-order system can capture more than 90% of the output energy while with $\ell_{0.99} = 4$ states the level 99% is exceeded for the one PHX model whereas the three PHX model is only slightly below that level and requires $\ell_{0.99} = 5$ states.

Fig. 7.3 allows to evaluate the actual quality of the output approximation. It plots the average temperature in the medium $Z(t) = \overline{Q}^M(t)$ against time and compares that system output of the original system (solid blue line) with the approximation $\tilde{Z}(t)$ from the reduced-order model (brown, orange, red lines) for $\ell = 1, 2, 4$. The figures also show the inlet temperature $Q^I(t)$ (black dotted line) which are constant and equal to $Q_C^I = 40^\circ\text{C}$ during charging (light red region) and $Q_D^I = 5^\circ\text{C}$ during discharging (light blue region), respectively. The figure shows that both for one and three PHXs, the reduced-order system captures well the input-output behaviour of the original high-dimensional system already

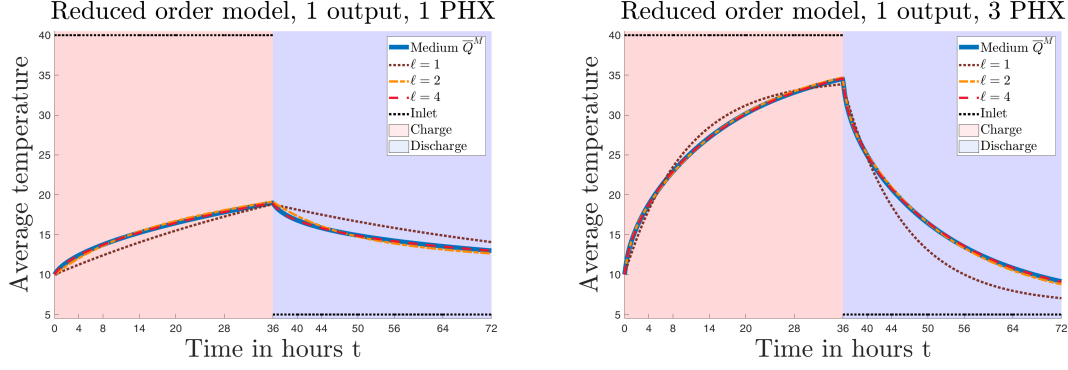


Fig. 7.3 Model with one output $Z = \bar{Q}^M$: Approximation of the output for $\ell = 1, 2, 4$. Left: one PHX , Right three PHXs.

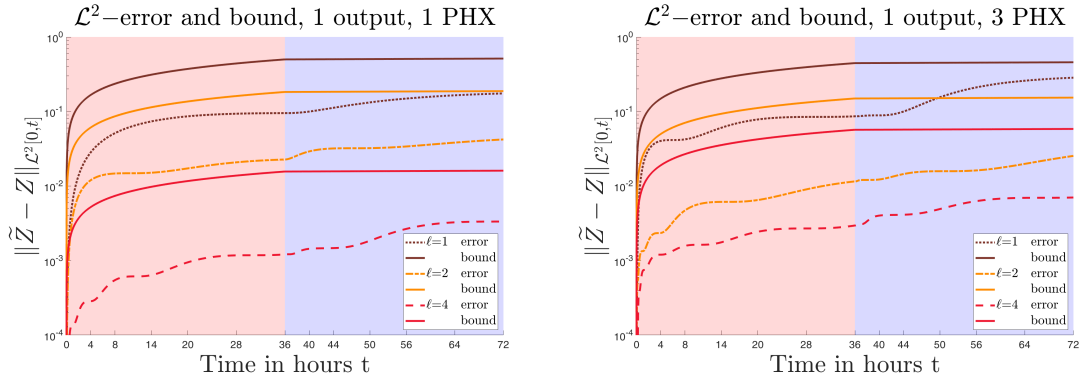


Fig. 7.4 Model with one output $Z = \bar{Q}^M$: \mathcal{L}_2 -error and error bound for $\ell = 1, 2, 4$. Left: one PHX , Right three PHXs.

for $\ell \geq 2$. For $\ell = 1$ the approximation is less good as expected in view of the low value of the selection criterion (see Fig. 7.2).

Finally, Fig. 7.4 plots the \mathcal{L}_2 -error $\|Z - \tilde{Z}\|_{\mathcal{L}_2(0,t)}$ against time t and compares with the associated error bound given in Theorem 6.17 for $\ell = 1, 2, 4$. Note that both quantities are non-decreasing in t . The error bounds grow less during discharging since here the growth of the \mathcal{L}_2 -norm of the input g is smaller due to the smaller inlet temperature Q^I , see Theorem 6.17. As expected from that theorem, the error bounds decrease with ℓ and this is also the case for the actual error.

The next examples will show that the number of states needed to capture well the input-output behavior of the system may increase considerably if we add more aggregated characteristics to the system output.

7.3 Two Aggregated Characteristics: \bar{Q}^M, \bar{Q}^F

In this example we add to the system output the average temperature of the PHX fluid leading to the two-dimensional output $Z = (\bar{Q}^M, \bar{Q}^F)^\top$. Since in the analogous system \bar{Q}^F is used as inlet temperature we now can include also waiting periods between periods of charging and discharging allowing the storage to mitigate saturation effects. For time horizon $T = 72$ hours we divide the simulation time interval $[0, T]$ into charging, discharging and waiting periods with

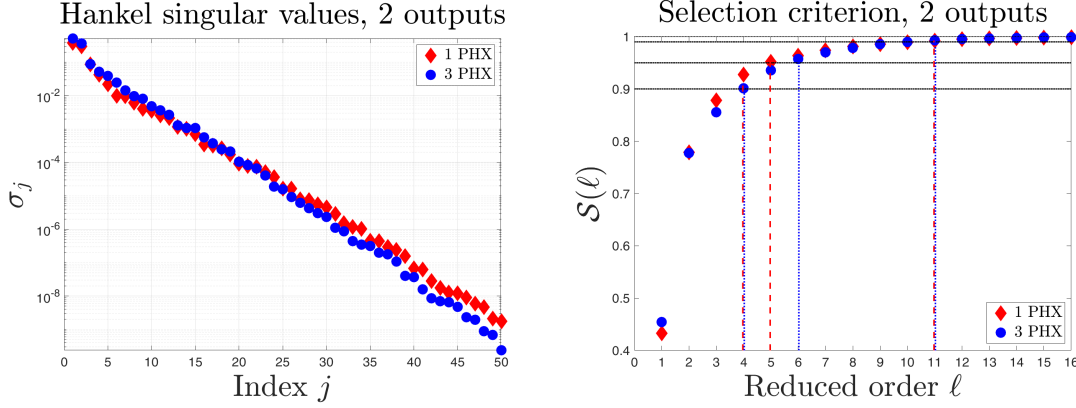


Fig. 7.5 Model with two outputs $Z = (\bar{Q}^M, \bar{Q}^F)^\top$:

Left: first 50 largest Hankel singular values, Right: selection criterion.

$$\begin{aligned} I_C &= [0, 4] \cup [8, 14] \cup [20, 28], & \text{charging,} \\ I_D &= [36, 40] \cup [44, 50] \cup [56, 64], & \text{discharging,} \\ I_W &= [0, 72] \setminus (I_C \cup I_D), & \text{waiting,} \end{aligned}$$

which are also depicted in Fig. 7.6. The two-dimensional input function g is defined as

$$g(t) = (Q^I(t), Q^G(t))^\top \text{ with } Q^I(t) = \begin{cases} Q_C^I = 40^\circ\text{C} & \text{for } t \in I_C \text{ (charging),} \\ Q_D^I = 5^\circ\text{C} & \text{for } t \in I_D \text{ (discharging),} \\ \bar{Q}^F(t) & \text{for } t \in I_W \text{ (waiting).} \end{cases} \quad (7.1)$$

Here, the inlet temperature $Q^I(t)$ is the piece-wise constant during charging and discharging but time-dependent and equal to $\bar{Q}^F(t)$ during waiting periods. Again the underground temperature is constant with $Q^G(t) = 15^\circ\text{C}$. The two rows of the $2 \times n$ output matrix C are C^M and C^F which are given in our companion paper [38, Sec. 4].

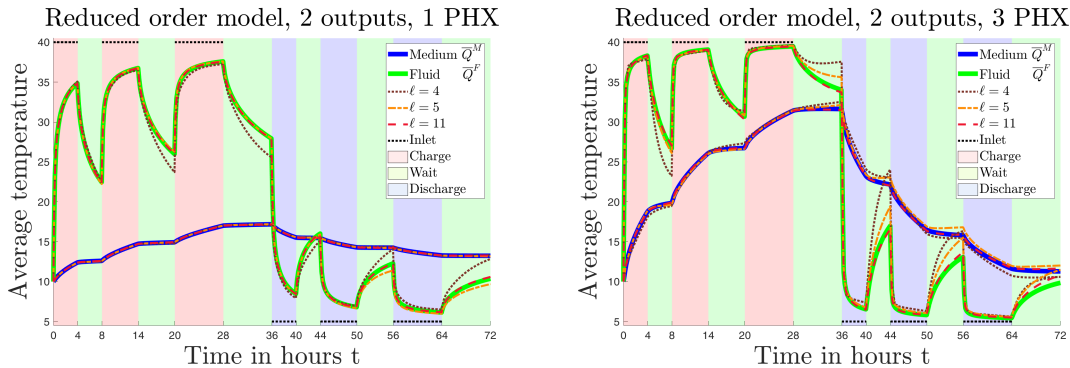


Fig. 7.6 Model with two outputs $Z = (\bar{Q}^M, \bar{Q}^F)^\top$: Approximation of the output for $\ell = 4, 5, 11$. Left: one PHX, Right three PHXs.

Fig. 7.5 depicts in the left panel the first 50 largest Hankel singular values whereas the right panel shows the selection criteria (red for 1 PHX and blue for 3 PHXs). For the first 50 singular values we observe for both models that they are all distinct and decrease by 9 orders of magnitude. As in the example with a single output the first 20 singular values decrease faster for the model with one PHX than for the 3 PHX model. The

selection criterion for the model with one PHX is for all $\ell \geq 2$ larger than for 3 PHXs. From Fig. 7.5 and also from the minimal reduced orders reported in Table 7.2 it can be seen that a reduced-order system with $\ell_{0.9} = 4$ states can capture more than 90% of the output energy of the original system. For the level threshold 95% the one PHX model requires $\ell_{0.95} = 5$ states while for the three PHX model $\ell_{0.95} = 6$ states are needed. In both cases the level of 99% is exceeded for the first time for $\ell_{0.99} = 11$. Hence, for dimension $\ell \geq 11$ an almost perfect approximation of the input-output behavior can be expected.

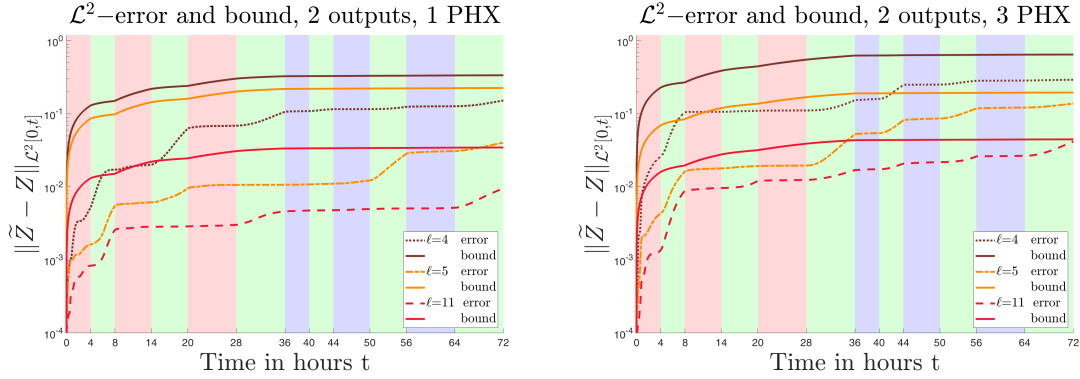


Fig. 7.7 Model with two outputs $Z = (\bar{Q}^M, \bar{Q}^F)^\top$: \mathcal{L}_2 -error and error bound for $\ell = 4, 5, 11$. Left: one PHX, Right three PHXs.

For the evaluation of the actual quality of the output approximation we plot in Fig. 7.6 the output variables of the original and reduced-order system against time. The average temperatures $Z_1(t) = \bar{Q}^M(t)$ and $Z_2(t) = \bar{Q}^F(t)$ in the medium and fluid are drawn as solid blue and green lines, respectively, and its approximations as brown, orange and red lines for $\ell = 4, 5, 11$. Further, the inlet temperature $Q^I(t)$ during the charging and discharging periods is shown as black dotted line. The figures show that the approximation of \bar{Q}^M is better than for \bar{Q}^F . A possible explanation is that \bar{Q}^M is an average of the spatial temperature distribution over the quite large subdomain \mathcal{D}^M (medium) while for \bar{Q}^F the temperature is averaged only over the much smaller subdomain \mathcal{D}^F of the PHX fluid. Further, the temporal variations of \bar{Q}^F are much larger than those of \bar{Q}^M due to the impact of the changing inlet temperature during charging, discharging and waiting. Errors are more pronounced during waiting periods than during charging and discharging. For the three PHX model the pointwise errors are slightly larger. As noted above, for $\ell = 11$ the selection criterion exceeds 99% and now the approximation errors are almost negligible. This was also observed for $\ell > 11$.

Fig. 7.7 plots for the reduced orders ℓ considered above the \mathcal{L}_2 -error $\|Z - \tilde{Z}\|_{\mathcal{L}_2(0,t)}$ against time t together with the error bounds from Theorem 6.17. This allows an alternative evaluation of the approximation quality. As expected, the error bounds and also the actual errors decrease with ℓ . While the error bounds increase more during the charging periods due to the larger norm of the input g caused by the higher inlet temperature the actual error increase more during the waiting periods. This corresponds to the above observed larger errors in the output approximation in during these periods.

7.4 Three Aggregated Characteristics I: $\bar{Q}^M, \bar{Q}^F, \bar{Q}^O$

This example extends the example considered in Sec. 7.3 by adding a third variable to the system output which is the average temperature at the PHX outlet, i.e., we consider the three-dimensional output $Z = (\bar{Q}^M, \bar{Q}^F, \bar{Q}^O)^\top$. The outlet temperature is needed if the geothermal storage is embedded into a residential system. Then the management of the heating system and the interaction between the geothermal and the internal buffer storage rely on the knowledge of \bar{Q}^O . Further, the difference $Q^I(t) - \bar{Q}^O(t)$ between inlet and outlet temperature is the key quantity for the quantification of the the amount of heat injected to or withdrawn from the storage due to convection of the fluid in the PHX, we refer to Eq. (4.2) and the explanations in Subsec. 4.2.

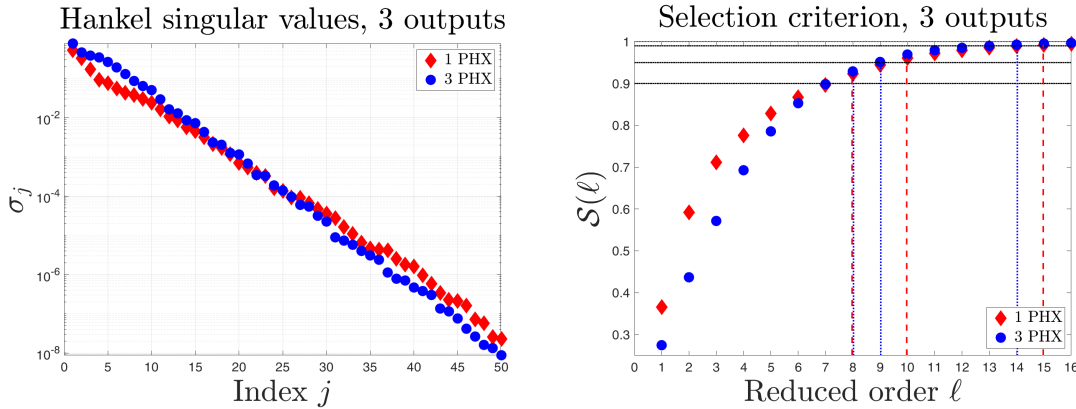


Fig. 7.8 Model with three outputs $Z = (\bar{Q}^M, \bar{Q}^F, \bar{Q}^O)^\top$:
Left: first 50 largest Hankel singular values, Right: selection criterion.

The setting is analogous to Subsec. 7.3. The input function g is given in (7.1) and the $3 \times n$ output matrix C is formed by the three rows C^M, C^F, C^O which are given in our companion paper [38, Sec. 4].

Fig. 7.8 shows as in the previous experiments in the left panel the first 50 largest Hankel singular values whereas the right right panel shows the selection criteria. For the first 50 singular values we observe for both models that they are all distinct and decrease by 8 orders of magnitude which is slightly less than for the case of only two outputs. As in the examples with one and two outputs the first 20 singular values decrease faster for the model with one PHX than for the 3 PHX model. The selection criterion for the model with one PHX is for $\ell \leq 6$ larger than for 3 PHXs and for $\ell \geq 7$ slightly smaller. Table 7.2 shows that for reaching threshold levels of $\alpha = 90\%, 95\%, 99\%$ in the one PHX case $\ell_\alpha = 8, 10, 15$ states are required while for three PHXs one needs $\ell_\alpha = 8, 9, 14$ states, respectively. Thus, for dimension $\ell \geq 15$ an almost perfect approximation of the input-output behavior can be expected. Note that in the previous experiment with two outputs (without outlet temperature) reaching the above thresholds requires about 4 to 5 states less.

In Fig. 7.9 we plot the output variables of the original and reduced-order system against time. The top panels show the average temperatures $Z_1(t) = \bar{Q}^M(t)$ and $Z_2(t) = \bar{Q}^F(t)$ in the medium and fluid which are drawn as solid blue and green lines, respectively. The bottom panels depict the average temperature at the outlet $Z_3(t) = \bar{Q}^O(t)$ by a solid green line. The reduced-order approximations are drawn for $\ell = 8, 10, 15$. As in the previous experiments with two outputs it can be observed that the approximation of \bar{Q}^M is better than for \bar{Q}^F .

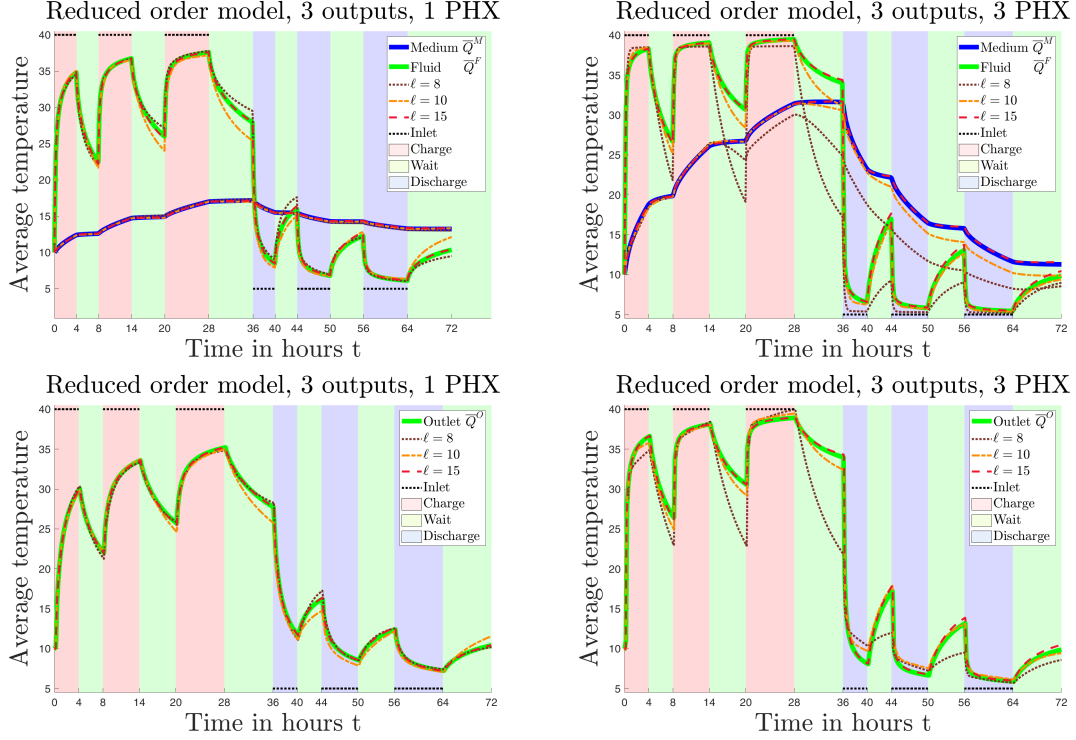


Fig. 7.9 Model with three outputs $Z = (\bar{Q}^M, \bar{Q}^F, \bar{Q}^O)^\top$: Approximation of the output for $\ell = 8, 10, 15$.

Top: Average temperatures in the medium \bar{Q}^M and the fluid \bar{Q}^F ,

Bottom: Average temperature at the outlet \bar{Q}^O ,

Left: one PHX, Right three PHXs.

The approximation errors for the outlet temperature \bar{Q}^O are quite similar to the errors for the fluid temperature. Note that the outlet temperature represents an average of the spatial temperature distribution over the quite small subdomain \mathcal{D}^O on the boundary which is still smaller than the subdomain \mathcal{D}^F over which the average is taken for the fluid temperature \bar{Q}^F . Both, the fluid and the outlet temperature show much larger temporal variations than the temperature in medium \bar{Q}^M . Again, errors are more pronounced during waiting periods than during charging and discharging and for the three PHX model the pointwise errors are larger than for the one PHX model. For $\ell \geq 15$ states the selection criterion is above 99% and the approximation errors are almost negligible.

Fig. 7.9 also shows that the average temperatures of the fluid and at the outlet pipe, \bar{Q}^M and \bar{Q}^O , exhibit almost the same pattern during the charging, discharging and waiting periods. Hence, knowing the average fluid temperature one can simply predict the outlet temperature and remove \bar{Q}^O from the output variables. Then we are back in the setting of the two output experiment in Subsec. 7.3 and need 4 to 5 states less to capture the input-output behaviour with the same approximation quality. Below in Subsec. 7.5 we consider a model where instead of removing \bar{Q}^O from the output this quantity is replaced by the average bottom temperature \bar{Q}^B leading again to a model with three outputs.

An alternative evaluation of the approximation quality can be derived from Fig. 7.10 which plots for the reduced orders ℓ considered above the \mathcal{L}_2 -error $\|Z - \tilde{Z}\|_{\mathcal{L}_2(0,t)}$ against time t together with the error bounds from Theorem 6.17. The results are similar to Fig. 7.7 and we refer for the interpretation to the end of the previous subsection.

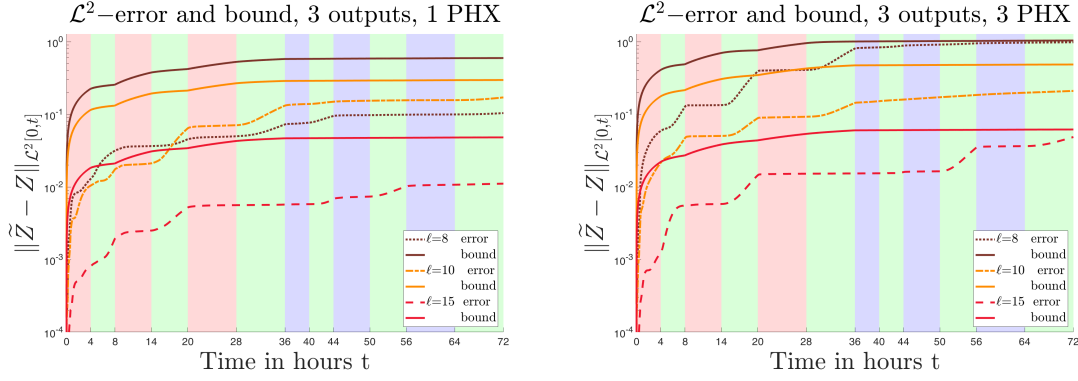


Fig. 7.10 Model with three outputs $Z = (\bar{Q}^M, \bar{Q}^F, \bar{Q}^O)^\top$: \mathcal{L}_2 -error and error bound for $\ell = 8, 10, 15$. Left: one PHX, Right three PHXs.

7.5 Three Aggregated Characteristics II: $\bar{Q}^M, \bar{Q}^F, \bar{Q}^B$

As already announced above in this experiment we again consider a model with three outputs but instead of the outlet temperature \bar{Q}^O now the third output is the average temperature at the bottom boundary \bar{Q}^B . Hence, the output is $Z = (\bar{Q}^M, \bar{Q}^F, \bar{Q}^B)^\top$. We recall that the bottom boundary is open and not insulated and the temperature \bar{Q}^B is of crucial importance for the quantification of gains and losses of thermal energy resulting from the heat transfer to the underground of the geothermal storage. We refer to Eq. (4.3) and the explanations in Subsec. 4.2 and the Robin boundary condition (2.3) modeling that heat transfer from the storage to the underground.

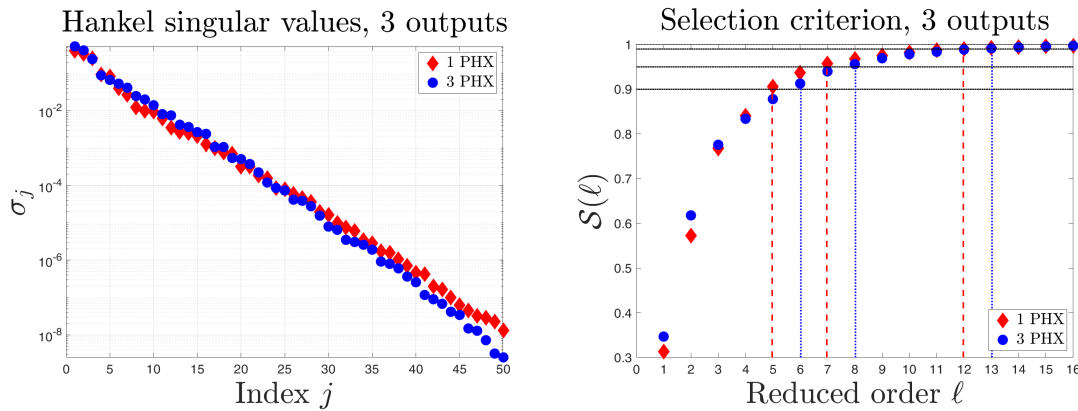


Fig. 7.11 Model with three outputs $Z = (\bar{Q}^M, \bar{Q}^F, \bar{Q}^B)^\top$: Left: first 50 largest Hankel singular values, Right: selection criterion.

The setting is analogous to Subsec. 7.3. The input function g is given in (7.1) and the $3 \times n$ output matrix C is formed by the four rows C^M, C^F, C^B which are given in our companion paper [38, Sec. 4].

Fig. 7.11 shows in the left panel the first 50 largest Hankel singular values whereas the right right panel shows the selection criteria. For both PHX models the first 50 singular values are distinct and decrease by more than 8 orders of magnitude which is only slightly less than for the case of two outputs. As in the previous experiments the first 20 singular values decrease faster for the model with one PHX than for the 3 PHX model. The selection criterion for the model with one PHX is for $\ell \leq 3$ smaller than for 3 PHXs and for $\ell \geq 4$ slightly

larger. From the figure and also from Table 7.2 it can be seen that for reaching threshold levels of $\alpha = 90\%, 95\%, 99\%$ in the one PHX case $\ell_\alpha = 5, 7, 12$ states are required while for three PHXs one needs $\ell_\alpha = 6, 8, 13$ states, respectively. Thus, for dimension $\ell \geq 13$ an almost perfect approximation of the input-output behavior can be expected.

A comparison with the two-output model in Subsec. 7.3 with output $Z = (\bar{Q}^M, \bar{Q}^F)^\top$ shows that the additional third output variable \bar{Q}^B requires only one or two more state variables to ensure the same approximation quality. However, the three-output model considered above in Subsec. 7.4 where the third output is the average outlet temperature \bar{Q}^O requires two or three states more in the reduced-order system to ensure the same approximation quality. This shows that \bar{Q}^B is much easier to reconstruct by a reduced-order model than \bar{Q}^O . An explanation is that for \bar{Q}^O the spatial temperature distribution is averaged over the subdomain \mathcal{D}^O which is much smaller than the corresponding domain \mathcal{D}^B over which the average is taken for \bar{Q}^B . Further, due to charging and discharging via the PHXs the outlet temperature shows much larger temporal variations than the temperature at the bottom \bar{Q}^M .

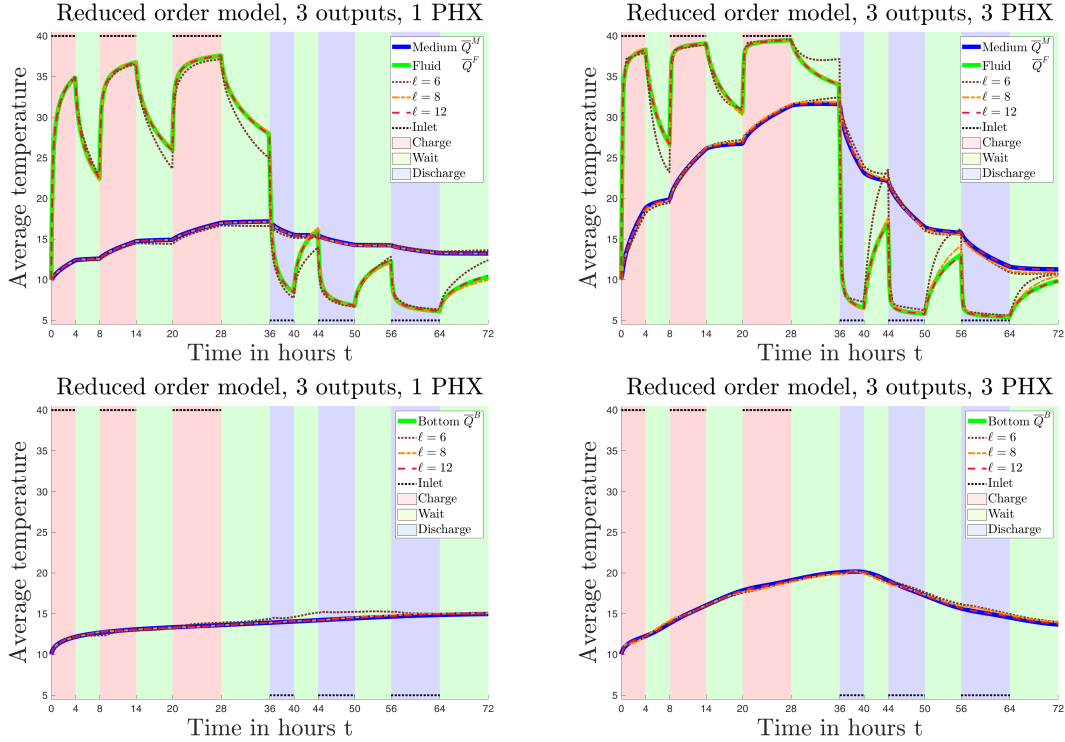


Fig. 7.12 Model with three outputs $Z = (\bar{Q}^M, \bar{Q}^F, \bar{Q}^B)^\top$: Approximation of the output for $\ell = 6, 8, 12$.

Top: Average temperatures in the medium \bar{Q}^M and the fluid \bar{Q}^F ,

Bottom: Average bottom temperature \bar{Q}^B ,

Left: one PHX, Right three PHXs.

Fig. 7.12 shows the output variables of the original and reduced-order system which are plotted against time. In the top panels the average temperatures $Z_1(t) = \bar{Q}^M(t)$ and $Z_2(t) = \bar{Q}^F(t)$ in the medium and fluid are drawn as solid blue and green lines, respectively. The bottom panel depicts the average temperature at the bottom boundary \bar{Q}^B by a blue solid line. The reduced-order approximations as drawn for $\ell = 6, 8, 12$.

As in the previous experiments the approximation of \bar{Q}^M is much better than for \bar{Q}^F . The approximation of the third output variable \bar{Q}^B is quite good although it represents

an average of the spatial temperature distribution over the rather small subdomain \mathcal{D}^B at the bottom boundary. Possible explanations are the relatively small temporal fluctuations of that quantity and the large distance of the bottom boundary to the PHXs where the charging and discharging generates large temporal and spatial fluctuations.

In Fig. 7.13 we show for the reduced orders ℓ considered above the \mathcal{L}_2 -error $\|\tilde{Z} - Z\|_{\mathcal{L}_2(0,t)}$ which plotted against time t together with the error bounds from Theorem 6.17. The results are similar to Fig. 7.7 and we refer for the interpretation to the end of Subsec. 7.3. Fig. 7.13:

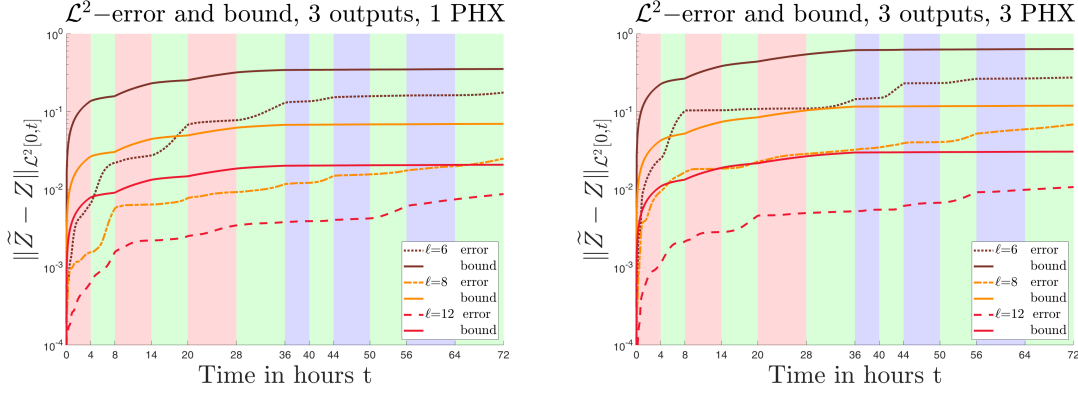


Fig. 7.13 Model with three outputs $Z = (\bar{Q}^M, \bar{Q}^F, \bar{Q}^B)^\top$: \mathcal{L}_2 -error and error bound for $\ell = 6, 8, 12$. Left: one PHX, Right three PHXs.

7.6 Four Aggregated Characteristics: $\bar{Q}^M, \bar{Q}^F, \bar{Q}^O, \bar{Q}^B$

In this last experiment the output contains all of four aggregated characteristics appearing in the above experiments and is given by $Z = (\bar{Q}^M, \bar{Q}^F, \bar{Q}^O, \bar{Q}^B)^\top$.

The setting is analogous to Subsec. 7.3. The input function g is given in (7.1) and the $4 \times n$ output matrix C is formed by the four rows C^M, C^F, C^O, C^B which are given in our companion paper [38, Sec. 4].

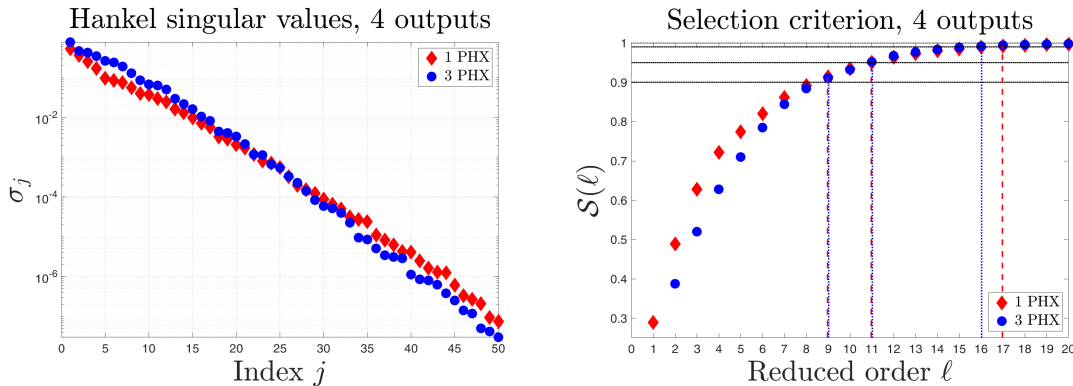


Fig. 7.14 Model with four outputs $Z = (\bar{Q}^M, \bar{Q}^F, \bar{Q}^O, \bar{Q}^B)^\top$: Left: first 50 largest Hankel singular values, Right: selection criterion.

Fig. 7.14 shows in the left panel the first 50 largest Hankel singular values whereas the right right panel shows the selection criteria. For both PHX models the first 50 singular

values are distinct and decrease by almost 8 orders of magnitude which is only slightly less than for the case of three outputs. As in the previous experiments the first 20 singular values decrease faster for the model with one PHX than for the 3 PHX model. The selection criterion for the model with one PHX is for $\ell \leq 10$ larger than for 3 PHXs and for $\ell \geq 11$ slightly smaller. From the figure and also from Table 7.2 it can be seen that for reaching threshold levels of $\alpha = 90\%, 95\%, 99\%$ in the one PHX case $\ell_\alpha = 9, 11, 17$ states are required while for three PHXs one needs $\ell_\alpha = 9, 11, 16$ states, respectively. Thus, for dimension $\ell \geq 17$ an almost perfect approximation of the input-output behavior can be expected. A comparison with the three output model in Subsec. 7.4 with output $Z = (\bar{Q}^M, \bar{Q}^F, \bar{Q}^O)^\top$ shows that the additional fourth output variable \bar{Q}^B requires only one or two more state variables to ensure the same approximation quality. This corresponds to our previous observations for the augmentation of the output $Z = (\bar{Q}^M, \bar{Q}^F)^\top$ of the model considered in Subsec. 7.3 by adding as third output the average bottom temperature \bar{Q}^B , see Subsec. 7.5. There the minimal reduced orders ℓ_α also increase only by one or two.

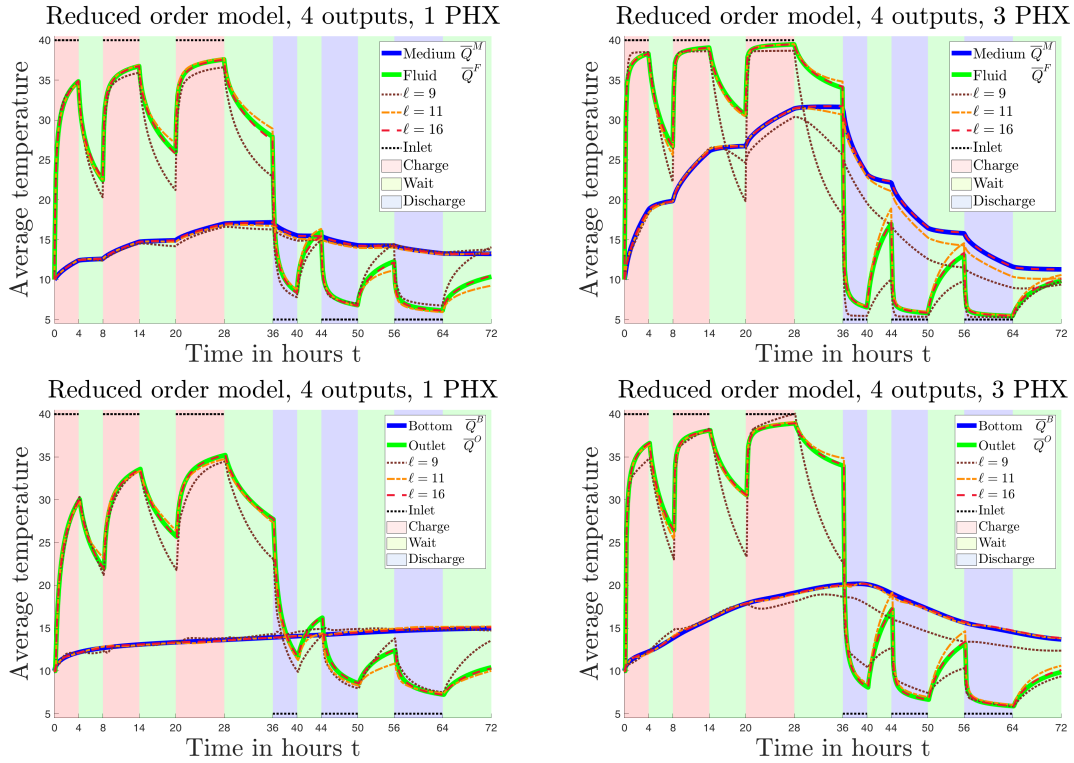


Fig. 7.15 Model with four outputs $Z = (\bar{Q}^M, \bar{Q}^F, \bar{Q}^O, \bar{Q}^B)^\top$: Approximation of the output for $\ell = 9, 11, 16$.
Top: Average temperatures in the medium \bar{Q}^M and the fluid \bar{Q}^F ,
Bottom: Average temperatures at the outlet \bar{Q}^O and the bottom boundary \bar{Q}^B ,
Left: one PHX, Right three PHXs.

Fig. 7.15 depicts the output variables of the original and reduced-order system which are plotted against time. In the top panels the average temperatures $Z_1(t) = \bar{Q}^M(t)$ and $Z_2(t) = \bar{Q}^F(t)$ in the medium and fluid are drawn as solid blue and green lines, respectively. The bottom panel shows the average temperatures at the outlet $Z_3(t) = \bar{Q}^O(t)$ and at the bottom boundary \bar{Q}^B by a blue and green line, respectively. The reduced-order approximations are drawn for $\ell = 9, 11, 16$.

The results for the first three outputs $\bar{Q}^M, \bar{Q}^F, \bar{Q}^O$ are similar to the experiment with those three outputs considered in Subsec. 7.4. The approximation of the fourth output variable \bar{Q}^B is quite good and comparable to the results in Subsec. 7.5. For the model with 3 PHXs we notice some visible errors for the smallest order $\ell = 9$.

Finally, Fig. 7.10 shows for the reduced orders ℓ considered above the \mathcal{L}_2 -error $\|\tilde{Z} - Z\|_{\mathcal{L}_2(0,t)}$ which plotted against time t together with the error bounds from Theorem 6.17. The results are similar to Fig. 7.7 and we refer for the interpretation to the end of Subsec. 7.3.

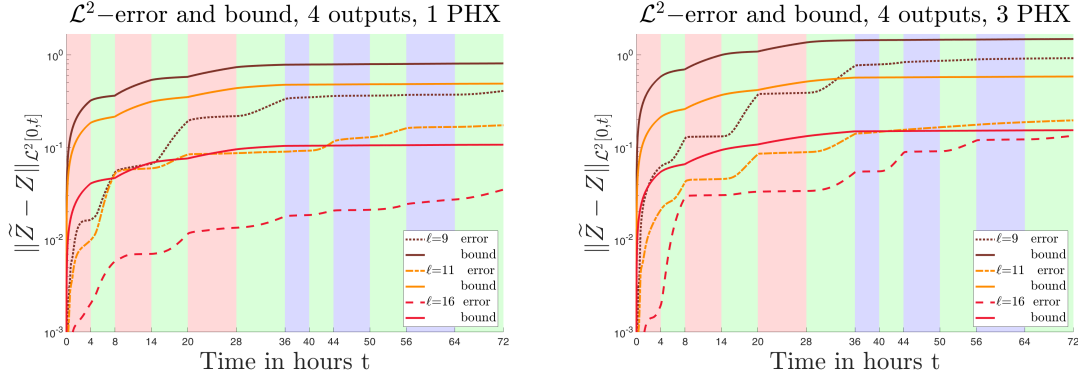


Fig. 7.16 Model with four outputs $Z = (\bar{Q}^M, \bar{Q}^F, \bar{Q}^O, \bar{Q}^B)^\top$: \mathcal{L}_2 -error and error bound for $\ell = 9, 11, 16$. Left: one PHX, Right three PHXs.

8 Conclusion

In this paper we have considered the approximate description of the input-output behavior of a geothermal storage by a low-dimensional system of linear ODEs. Starting point was the mathematical modeling of the spatio-temporal temperature distribution in a two-dimensional cross section of the storage by a linear heat equation with a convection term. By semi-discretization of that PDE w.r.t. spatial variables we obtained a high-dimensional system of non-autonomous ODEs. The latter was approximated by an analogous LTI system. Reduced-order models in which the state dynamics is described by a low-dimensional system of linear ODEs were derived by the Lyapunov balanced truncation method. In our numerical experiments we considered aggregated characteristics describing the input-output behavior of the storage which are required for the operation of the geothermal storage within a residential heating system. The results show that it is possible to obtain quite accurate approximations from reduced-order systems with only a few state variables. This allows to treat the cost-optimal management of residential heating systems as a decision making problem under uncertainty which mathematically can be formulated as a stochastic optimal control problem. Results on that will be published in an forthcoming paper.

A List of Notations

$Q = Q(t, x, y)$	temperature in the geothermal storage
T	finite time horizon
l_x, l_y, l_z	width, height and depth of the storage
$\mathcal{D} = (0, l_x) \times (0, l_y)$	domain of the geothermal storage
$\mathcal{D}^F, \mathcal{D}^M$	domain inside and outside the pipes
$\mathcal{D}^J = \underline{\mathcal{D}}^J \cup \overline{\mathcal{D}}^J$	interface between the pipes and the medium (dry soil)
$\partial\mathcal{D}$	boundary of the domain
$\partial\mathcal{D}^I, \partial\mathcal{D}^O$	inlet and outlet boundaries of the pipe
$\partial\mathcal{D}^L, \partial\mathcal{D}^R, \partial\mathcal{D}^T, \partial\mathcal{D}^B$	left, right, top and bottom boundaries of the domain
\mathcal{N}_*	subsets of index pairs for grid points
$\mathcal{K}, \overline{\mathcal{K}}$	mappings $(i, j) \mapsto l$ of index pairs to single indices
$v = v_0(t)(v^x, v^y)^\top$	time-dependent velocity vector,
\bar{v}_0	constant velocity during pumping
c_p^F, c_p^M	specific heat capacity of the fluid and medium
ρ^F, ρ^M	mass density of the fluid and medium
κ^F, κ^M	thermal conductivity of the fluid and medium
a^F, a^M	thermal diffusivity of the fluid and medium
λ^G	heat transfer coefficient between storage and underground
Q_0	initial temperature distribution of the geothermal storage
Q^G	underground temperature
Q^I, Q_C^I, Q_D^I	inlet temperature of the pipe, during charging and discharging,
\bar{Q}^M, \bar{Q}^F	average temperature in the storage medium and fluid
\bar{Q}^O, \bar{Q}^B	average temperature at the outlet and bottom boundary
G^*	gain of thermal energy in a certain subdomain
I_C, I_W, I_D	time interval for charging, waiting, discharging periods
$\nabla, \Delta = \nabla \cdot \nabla$	gradient, Laplace operator
PHX	pipe heat exchanger
$N_x, N_y,$	number of grid points in x, y -direction
h_x, h_y	step size in x and y -direction
n_P	number of pipes
\mathbf{n}	outward normal to the boundary $\partial\mathcal{D}$
n	dimension of vector Y
ℓ	dimension of the reduced-order system
\mathbb{I}_n	$n \times n$ identity matrix
A, B, C	$n \times n$ system matrix, $n \times m$ input matrix, $n_0 \times n$ output matrix of original system
$\bar{A}, \bar{B}, \bar{C}$	$n \times n$ system matrix, $n \times m$ input matrix, $n_0 \times n$ output matrix of transformed original system
$\tilde{A}, \tilde{B}, \tilde{C}$	$\ell \times \ell$ system matrix, $\ell \times m$ input matrix, $n_0 \times \ell$ output matrix of the reduced-order system
D^\pm, A_L, A_M, A_R	block matrices of matrix A
Y, \bar{Y}	n dimensional state of original and transformed original system
\tilde{Y}	ℓ dimensional state of reduced-order system
Z	n_o dimensional output of original system
\tilde{Z}	n_o dimensional output of reduced-order system
g	input variable of the system
$\mathcal{G}_C, \mathcal{G}_O$	controllability and observability Gramians

$\overline{\mathcal{G}}_C, \overline{\mathcal{G}}_O$	transformed controllability and observability Gramians
\mathcal{T}	invariant transformation
$\sigma_i > 0$	Hankel singular values
Σ	diagonal matrix of Hankel singular values
U, L	upper/ lower triangular matrix from Cholesky decomp. of $\mathcal{G}_C/\mathcal{G}_O$
K	orthogonal matrix from the eigenvalue decomposition of $U^\top \mathcal{G}_O U$
W, V	unitary matrices from the singular value decomposition
$\mathcal{S}(\ell)$	selection criterion
$\mathcal{L}_2(0, t)$	set of square integrable functions on $[0, t]$

B Proofs

B.1 Proof of Lemma 6.1

Using $\bar{Y} = \mathcal{T}Y$ and $Y = \mathcal{T}^{-1}\bar{Y}$ we get $\dot{Y} = \mathcal{T}^{-1}\dot{\bar{Y}}$. Substituting into (6.1) implies

$$\mathcal{T}^{-1}\dot{\bar{Y}}(t) = A\mathcal{T}^{-1}\bar{Y}(t) + Bg(t), \quad Z(t) = C\mathcal{T}^{-1}\bar{Y}(t)$$

Left-multiplication of the state equation by \mathcal{T} leads to

$$\mathcal{T}\mathcal{T}^{-1}\dot{\bar{Y}}(t) = \mathcal{T}A\mathcal{T}^{-1}\bar{Y}(t) + \mathcal{T}Bg(t), \quad Z(t) = C\mathcal{T}^{-1}\bar{Y}(t).$$

from which we obtain a transformed system $\dot{\bar{Y}}(t) = \bar{A}\bar{Y}(t) + \bar{B}g(t)$, $Z(t) = \bar{C}\bar{Y}(t)$ with $\bar{A} = \mathcal{T}A\mathcal{T}^{-1}$, $\bar{B} = \mathcal{T}B$ and $\bar{C} = C\mathcal{T}^{-1}$.

B.2 Proof of Theorem 6.8

We first prove $\mathcal{E}_O(y) = y^\top \mathcal{G}_O y$. For zero input $g = 0$ and initial state $Y(0) = y$ the state equation of system (6.1) has a unique solution $Y(t) = e^{At}y$ and the output is given by $Z(t) = CY = Ce^{At}y$ for $t \geq 0$. Hence

$$y^\top \mathcal{G}_O y = \int_0^\infty y^\top e^{A^\top t} C^\top C e^{At} y dt = \int_0^\infty (y e^{At} C)^\top C e^{At} y dt = \int_0^\infty \|C e^{At} y\|_2^2 dt = \int_0^\infty \|Z(t)\|_2^2 dt.$$

The proof of $\mathcal{E}_C(y) = y^\top \mathcal{G}_C^{-1} y$ can be derived from the results established in [36].

B.3 Proof of Theorem 6.9

The proof is derived from the one sketched in Antouslas [2, Proposition 4.27]. Assume that a system matrix A is stable, then we have:

$$\begin{aligned} A\mathcal{G}_C + \mathcal{G}_C A^\top &= \int_0^\infty \left(A e^{At} B B^\top e^{A^\top t} + e^{At} B B^\top e^{A^\top t} A^\top \right) dt = \int_0^\infty \frac{d}{dt} \left(e^{At} B B^\top e^{A^\top t} \right) dt \\ &= \lim_{T \rightarrow \infty} e^{AT} B B^\top e^{A^\top T} \Big|_0^T = \lim_{T \rightarrow \infty} e^{AT} B B^\top e^{A^\top T} - B B^\top = -B B^\top. \\ \mathcal{G}_O A + A^\top \mathcal{G}_O &= \int_0^\infty \left(e^{A^\top t} C^\top C e^{At} A + A^\top e^{A^\top t} C^\top C e^{At} \right) dt = \int_0^\infty \frac{d}{dt} \left(e^{A^\top t} C^\top C e^{At} \right) dt \\ &= \lim_{T \rightarrow \infty} e^{A^\top T} C^\top C e^{AT} \Big|_0^T = \lim_{T \rightarrow \infty} e^{A^\top T} C^\top C e^{AT} - C^\top C = -C^\top C \end{aligned}$$

B.4 Proof of Lemma 6.11

We follow the proof in Antouslas [2, Sec. 4.3]. Let $\bar{\mathcal{G}}_C$ and $\bar{\mathcal{G}}_O$ be the controllability and observability Gramians of the transformed system, respectively. Then $\bar{\mathcal{G}}_C$ satisfies the following Lyapunov equation:

$$0 = \bar{A} \bar{\mathcal{G}}_C + \bar{\mathcal{G}}_C \bar{A}^\top + \bar{B} \bar{B}^\top = \mathcal{T} A \mathcal{T}^{-1} \bar{\mathcal{G}}_C + \bar{\mathcal{G}}_C (\mathcal{T} A \mathcal{T}^{-1})^\top + \mathcal{T} B (\mathcal{T} B)^\top$$

Multiplying by \mathcal{T}^{-1} from left and by $\mathcal{T}^{-\top}$ from right gives

$$0 = A(\mathcal{T}^{-1} \bar{\mathcal{G}}_C \mathcal{T}^{-\top}) + (\mathcal{T}^{-1} \bar{\mathcal{G}}_C \mathcal{T}^{-\top}) A^\top + B B^\top$$

Comparing with the Lyapunov equation for the Gramian \mathcal{G}_C of the original system which reads as $0 = A \mathcal{G}_C + \mathcal{G}_C A^\top + B B^\top$ gives $\mathcal{G}_C = \mathcal{T}^{-1} \bar{\mathcal{G}}_C \mathcal{T}^{-\top}$ and finally $\bar{\mathcal{G}}_C = \mathcal{T} \mathcal{G}_C \mathcal{T}^\top$.

Similar reasoning gives $\bar{\mathcal{G}}_O = \mathcal{T}^{-\top} \mathcal{G}_O \mathcal{T}^{-1}$.

Substituting into the product of the transformed Gramians yields $\bar{\mathcal{G}}_C \bar{\mathcal{G}}_O = \mathcal{T} \mathcal{G}_C \mathcal{G}_O \mathcal{T}^{-1}$.

B.5 Proof of Theorem 6.13

We have to prove that the system is balanced under the transformation $\mathcal{T} = \Sigma^{\frac{1}{2}} K^\top U^{-1}$. For the Gramians of the transformed system, we obtain

$$\bar{\mathcal{G}}_C = \mathcal{T} \mathcal{G}_C \mathcal{T}^\top = \Sigma^{\frac{1}{2}} K^\top U^{-1} \mathcal{G}_C U^{-\top} K \Sigma^{\frac{1}{2}} = \Sigma^{\frac{1}{2}} K^\top U^{-1} U U^\top U^{-\top} K \Sigma^{\frac{1}{2}} = \Sigma^{\frac{1}{2}} K^\top K \Sigma^{\frac{1}{2}} = \Sigma^{\frac{1}{2}} \Sigma^{\frac{1}{2}} = \Sigma.$$

$$\bar{\mathcal{G}}_O = \mathcal{T}^{-\top} \mathcal{G}_O \mathcal{T}^{-1} = \Sigma^{-\frac{1}{2}} K^\top U^\top \mathcal{G}_O U K \Sigma^{-\frac{1}{2}} = \Sigma^{-\frac{1}{2}} K^\top K \Sigma^2 K^\top K \Sigma^{-\frac{1}{2}} = \Sigma^{-\frac{1}{2}} \Sigma^2 \Sigma^{-\frac{1}{2}} = \Sigma.$$

We used $\mathcal{G}_C = U U^\top$, $U^\top U^{-\top} = I_n = U^{-1} U$, $U^\top \mathcal{G}_O U = K \Sigma^2 K^\top$ and $K^\top K = I_n$.

Acknowledgements The authors thank Martin Bähr (DLR), Martin Redmann (Martin-Luther University Halle–Wittenberg), Olivier Menoukeu Pamen (University of Liverpool) and Gerd Wachsmuth (BTU Cottbus–Senftenberg) for valuable discussions that improved this paper.

P.H. Takam gratefully acknowledges the support by the German Academic Exchange Service (DAAD) within the project “PeStO – Perspectives in Stochastic Optimization and Applications”.

References

1. AMSALLEM, D., AND FARHAT, C. Stabilization of projection-based reduced-order models. *International Journal for Numerical Methods in Engineering* 91, 4 (2012), 358–377.
2. ANTOULAS, A. C. *Approximation of large-scale dynamical systems*. (2005), SIAM.
3. BÄHR, M., AND BREUSS, M. *Efficient Long-Term Simulation of the Heat Equation with Application in Geothermal Energy Storage. Mathematics*, (2022), vol. 10, p. 2309.
4. BÄHR, M., BREUSS, M., AND WUNDERLICH, R. Fast explicit diffusion for long-time integration of parabolic problems. In *International Conference of Numerical Analysis and Applied Mathematics (ICNAAM 2016)* (2017), vol. 1863, p. 410002.
5. BEATTIE C., GUGERCIN, S., AND MEHRMANN, V. Model reduction for systems with inhomogeneous initial conditions, *Systems & Control Letters* 99 (2017), 99–106.
6. BENNER, P., KÜRSCHNER, P., AND SAAK, J. Self-generating and efficient shift parameters in adi methods for large Lyapunov and sylvester equations. *Electronic Transactions on Numerical Analysis (ETNA)* 43 (2014), 142–162.
7. BENNER, P., LI, J.-R., AND PENZL, T. Numerical solution of large-scale Lyapunov equations, Riccati equations, and linear-quadratic optimal control problems. *Numerical Linear Algebra with Applications* 15, 9 (2008), 755–777.

8. BENNER, P., MEHRMANN, V., AND SORESENSEN, D. C. *Dimension reduction of large-scale systems*, vol. 45. (2005), Springer.
9. BENNER, P., AND QUINTANA-ORTÍ, E. S. Solving stable generalized Lyapunov equations with the matrix sign function. *Numerical Algorithms* 20, 1 (1999), 75–100.
10. BENNER, P., QUINTANA-ORTÍ, E. S., AND QUINTANA-ORTÍ, G. Balanced truncation model reduction of large-scale dense systems on parallel computers. *Mathematical and Computer Modelling of Dynamical Systems* 6, 4 (2000), 383–405.
11. BESSELINK, B., TABAK, U., LUTOWSKA, A., VAN DE WOUW, N., NIJMEIJER, H., RIXEN, D. J., HOCHSTENBACH, M., AND SCHILDERS, W. A comparison of model reduction techniques from structural dynamics, numerical mathematics and systems and control. *Journal of Sound and Vibration* 332, 19 (2013), 4403–4422.
12. BYERS, R., HE, C., AND MEHRMANN, V. The matrix sign function method and the computation of invariant subspaces. *SIAM Journal on Matrix Analysis and Applications* 18, 3 (1997), 615–632.
13. DARAGHMEH, A., HARTMANN, C., AND QATANANI, N. Balanced model reduction of linear systems with nonzero initial conditions: Singular perturbation approximation, *Applied Mathematics and Computation* 353 (2019), 295–307.
14. DAVIS, J.M., GRAVAGNE, I.A., JACKSON, B.J. AND MARKS II, R.J. Controllability, observability, realizability, and stability of dynamic linear systems. *Electronic Journal of Differential Equations*, 37 (2009), 1–32.
15. ENNS, D. F. Model reduction with balanced realizations: An error bound and a frequency weighted generalization. In *The 23rd IEEE Conference on Decision and Control* (1984), IEEE, pp. 127–132.
16. FREUND, R. W. Krylov-subspace methods for reduced-order modeling in circuit simulation. *Journal of Computational and Applied Mathematics* 123, 1-2 (2000), 395–421.
17. GLOVER, K. All optimal hankel-norm approximations of linear multivariable systems and their L^∞ -error bounds. *International Journal of Control* 39, 6 (1984), 1115–1193.
18. GOSEA, I. V., PETRECZKY, M., ANTOULAS, A. C., AND FITER, C. Balanced truncation for linear switched systems. *Advances in Computational Mathematics* 44, 6 (2018), 1845–1886.
19. GUELPA, E., AND VERDA, V. Thermal energy storage in district heating and cooling systems: A review. *Applied Energy* 252 (2019), 113474.
20. GUGERCIN, S., AND ANTOULAS, A. C. A survey of model reduction by balanced truncation and some new results. *International Journal of Control* 77, 8 (2004), 748–766.
21. HACKBUSCH, W. A sparse matrix arithmetic based on H-matrices. part I: Introduction to H-matrices. *Computing* 62, 2 (1999), 89–108.
22. HAMMARLING, S. J. Numerical solution of the stable, non-negative definite Lyapunov equation. *IMA Journal of Numerical Analysis* 2, 3 (1982), 303–323.
23. HEINKENSCHLOSS, M., REIS, T., AND ANTOULAS, A.C. Balanced truncation model reduction for systems with inhomogeneous initial conditions, *Automatica* 47 (2011), no. 3, 559–564.
24. HODEL, A. S., AND POOLLA, K. Parallel solution of large Lyapunov equations. *SIAM Journal on Matrix Analysis and Applications* 13, 4 (1992), 1189–1203.
25. JAIMOUKHA, I. M., AND KASENALLY, E. M. Krylov subspace methods for solving large Lyapunov equations. *SIAM Journal on Numerical Analysis* 31, 1 (1994), 227–251.
26. KITAPBAYEV, Y., MORIARTY, J., AND MANCARELLA, P. Stochastic control and real options valuation of thermal storage-enabled demand response from flexible district energy systems. *Applied Energy* 137 (2015), 823 – 831.
27. KÜRSCHNER, P. Balanced truncation model order reduction in limited time intervals for large systems. *Advances in Computational Mathematics* 44, 6 (2018), 1821–1844.
28. MEHRMANN, V., AND STYKEL, T. Balanced truncation model reduction for large-scale systems in descriptor form. In *Dimension Reduction of Large-Scale Systems*. Springer, 2005, pp. 83–115.
29. MOORE, B. Principal component analysis in linear systems: Controllability, observability, and model reduction. *IEEE transactions on automatic control* 26, 1 (1981), 17–32.
30. MULLIS, C., AND ROBERTS, R. Synthesis of minimum roundoff noise fixed point digital filters. *IEEE Transactions on Circuits and Systems* 23, 9 (1976), 551–562.
31. PENZL, T. A cyclic low-rank smith method for large sparse Lyapunov equations. *SIAM Journal on Scientific Computing* 21, 4 (1999), 1401–1418.

32. PERNEBO, L., AND SILVERMAN, L. Model reduction via balanced state space representations. *IEEE Transactions on Automatic Control* 27, 2 (1982), 382–387.
33. REDMANN, M. *Balancing Related Model Order Reduction Applied to Linear Controlled Evolution Equations with Lévy Noise*. PhD thesis, Otto-von-Guericke Universität Magdeburg, (2016).
34. SCHRÖDER, C., AND VOIGT, M. Balanced truncation model reduction with a priori error bounds for LTI systems with nonzero initial value, *Journal of Computational and Applied Mathematics* (2022), 114708.
35. SIMONCINI, V. A new iterative method for solving large-scale Lyapunov matrix equations. *SIAM Journal on Scientific Computing* 29, 3 (2007), 1268–1288.
36. STYKEL, T. *Analysis and numerical solution of generalized Lyapunov equations*. PhD thesis, Institut für Mathematik, Technische Universität, Berlin, (2002).
37. TAKAM, P. H., WUNDERLICH, R., AND PAMEN, O. M. Short-term behavior of a geothermal energy storage: Modeling and theoretical results. *arXiv preprint arXiv:2104.05005 [math.NA]* (2021).
38. TAKAM, P. H., WUNDERLICH, R., AND PAMEN, O. M. Short-term behavior of a geothermal energy storage: Numerical applications. *arXiv preprint arXiv:2104.05116 [math.NA]* (2021).
39. TOMBS, M.S., AND POSTLETHWAITE, I. Truncated balanced realization of a stable non-minimal state-space system. *International Journal of Control*, 46:4 (1987) 1319-1330.
40. VOLKWEIN, S. Proper orthogonal decomposition: Theory and reduced-order modelling. *Lecture Notes, University of Konstanz* 4, 4 (2013), 1–29.